The 2007 Stromboli eruption: event chronology and effusion rates using thermal infrared data

Calvari S.[(1)], Lodato L. [(1)], Steffke A. [(2)], Cristaldi A. [(1)], Harris A.J.L. [(3)], Spampinato L. [(1)], Boschi E. [(1)]

(1) Istituto Nazionale di Geofisica e Vulcanologia, sezione di Catania (INGV-CT), Piazza Roma 2, 95123 Catania, Italy
(2) HIGP/SOEST, University of Hawaii, 1680 East West Road, Honolulu, Hawaii, 96822, USA
(3) Laboratoire Magmas et Volcans, Université Blaise Pascal, 5 Rue Kessler, 63038 Clermont Ferrand, France

Abstract

Using thermal infrared images recorded by a permanent thermal camera network maintained on Stromboli volcano (Italy), together with satellite and helicopter-based thermal image surveys, we have compiled a chronology of the events and processes occurring before and during Stromboli's 2007 effusive eruption. These digital data also allow us to calculate the effusion rates and lava volumes erupted during the effusive episode. At the onset of the 2007 eruption, two parallel eruptive fissures developed within the North East crater, eventually breaching the NE flank of the summit cone and extending along the eastern margin of the Sciara del Fuoco. These fed a main effusive vent at 400 m a.s.l. to feed lava flows that extended to the sea. The effusive eruption was punctuated, on 15 March, by a paroxysm with features similar to the 5 April paroxysm that occurred during the 2002-03 effusive eruption. A total of between 3.2 x 10^6 m^3 and 11 x 10^6 m^3 of lava was erupted during the 2007 eruption over 34 days of effusive activity. More than half of this volume was emplaced during the first 5.5 days of the eruption. Although the 2007 effusive eruption had a comparable erupted volume to the previous (2002-03) effusive eruption, it had a shorter duration and thus a mean output rate (= total volume divided by eruption duration) that was one order of magnitude greater than the 2002-03 event (~2.4 m^3 s^{-1} compared with 0.32±0.28 m^3 s^{-1}). In this paper, we discuss similarities and differences between these two effusive events, and interpret the processes occurring in 2007 in terms of the recent dynamics witnessed at Stromboli.

1. Introduction

Typical eruptive activity at Stromboli (Aeolian Islands, Italy, Fig. 1a-b) consists of persistent, mildly explosive events occurring every 5 to 20 minutes. Typically, these Strombolian events erupt small volumes of ejecta to heights of between 150 and 300 m above the active vents [*Harris and Ripepe*, 2007a] (Fig. 1c-d). The summit crater area (the crater terrace) is an elliptical depression ~300 m long and ~50 m wide (Fig. 1c). The crater terrace is at ~750 m a.s.l., which places it ~170 m below Il Pizzo (918 m a.s.l., Fig. 1c). The crater terrace comprises three craters, whose geographic position has remained remarkably constant over at-least 100 years [e.g. *Washington*, 1917; *Calvari et al.*, 2005a, 2005b; *Harris and Ripepe*, 2007a]. Effusive eruptions at this volcano have a frequency of 5 to 15 years [*Barberi et al.*, 1993], with lava flows erupted during the last two millennia being confined to the Sciara del Fuoco (SDF), a collapse scar on the NW flank of the volcano (Fig. 1b-c).

Since 2001, the monitoring of effusive and explosive eruptions at Stromboli has increasingly involved use of thermal imagery obtained from hand-held thermal infrared cameras. Data collected from fixed stations and helicopter-based surveys have played four roles. First, they have allowed checking of the temperature variations at, as well as the number, position and morphology of active vents within the crater terrace [*Calvari et al.*, 2005a, 2005b; *Burton et al.*, 2008], as well as the location and opening of eruptive fractures [*Ripepe et al.*, 2009]. Second, they have allowed mapping of active lava flow fields and the development of lava flow features [*Calvari et al.,* 2006; *Lodato et al.*, 2007]. Third, they have been used to derive heat fluxes and effusion rates during effusive events [*Harris et al.*, 2005b; *Calvari et al.,* 2005a, 2005b; *Lodato et al.*, 2007]. Fourth, they have been used to study the eruption dynamics during persistent explosive activity [*Harris and Ripepe*, 2007a; *Patrick*, 2007; *Patrick et al.*, 2007; *Zanon et al.*, 2009], gas puffing [*Harris and Ripepe*, 2007b], and paroxysms [*Calvari et al.*, 2006; *Harris et al.*, 2008].

Thermal camera's were used for the first time during an effusive event at Stromboli during the 2002-03 eruption. This eruption produced a number of different phenomena such as tsunami [*Bonaccorso et al.*, 2003; *Tinti et al.*, 2005], sliding of portions of the SDF [*Tommasi et al.*, 2008], flank collapses and opening of fractures and eruptive vents [*Bonaccorso et al.*, 2003; *Calvari et al.*, 2005a, 2005b], paroxysmal explosive events [*Calvari et al.*, 2006; *Rosi et al.*, 2006; *Harris et al.*, 2008], and emplacement of compound lava flow fields on steep slopes [*Calvari et al.*, 2005a, 2005b; *Lodato et al.*, 2007; *Spampinato et al.*, 2008a]. The later stages of the eruption were characterized by low effusion rates (typically <1 m^3 s^{-1}; *Calvari et al.*, 2005a, 2005b; *Harris et al.*, 2005b*; Lodato et al.*, 2007] and a transition back to the typical strombolian activity experienced by Stromboli [*Ripepe et al.*, 2005]. As a result of the 2002-03 event, monitoring systems deployed on the volcano were significantly expanded to allow improved forecasting capabilities in the event of new and potentially dangerous eruptive events. Consequently, instrumentation was in place and operational at the onset of the 2007 effusive event.

The 2007 eruption began on 27 February 2007 and lasted 34 days until 2 April, and has previously been the topic of a Journal of Volcanogical and Geophysical Research special issue [*Scandone et al.*, 2009] in which *Barberi et al.* [2009] provided a chronological overview of events. In this paper, we discuss the dynamics of Stromboli's 2007 effusive eruption providing a chronology of the events based on qualitative and quantitative analyses of thermal infrared images recorded by fixed web-cameras operated by the Istituto Nazionale di Geofisica e Vulcanologia, sezione di Catania (INGV-CT). Lava effusion rate is also a key parameter when forecasting maximum lava flow length and estimating volcanic hazard [e.g., *Kilburn*, 1993; *Calvari and Pinkerton*, 1998; *Harris and Rowland*, 2009], as well as in assessing the depressurisation state and eruption mechanisms operating during an effusive eruption [e.g., *Wadge*, 1981; *Harris et al.*, 2000; *Rowland et al.*, 2003]. We thus also present effusion rates calculated from thermal images acquired using Forward Looking InfraRed spectrometer (FLIR) thermal infrared cameras, as well as those estimated using two satellite-based sensors: the Advanced Very High Resolution Radiometer (AVHRR) and MODerate resolution Imaging Spectroradiometer (MODIS).

2. The INGV-CT thermal camera monitoring system at Stromboli

During and following Stromboli's 2002-03 effusive eruption, the INGV-CT thermal monitoring system was greatly improved. As a result, during the 2007 effusive eruption, we were able to collect a high temporal

84 resolution thermal data set to allow assessment of the daily variation in eruptive events from the onset of the
85 eruption. Here, we describe the camera network installed on Stromboli, the instrument characteristics and
86 methodology, as well as use of helicopter- and satellite-based thermal imaging. All data were then used for
87 near-real-time thermal surveillance of the eruptive events.
88
89 *2.1. Web-camera network*
90
91 Prior to 2002, the INGV-CT camera network consisted of a visual camera located at Il Pizzo, a location at
92 918 m a.s.l. that overlooks the crater terrace (Fig. 1c). From this location the camera captured images for the
93 entire crater terrace (~170 m below the camera location) over a downward looking line of sight with a
94 camera-to-target distance of between 250 and 300 m (Fig. 1c-d). This enabled imaging of the explosive
95 events, the estimation of the height attained by the products to a maximum limit of ~200 m (the upper limit of
96 the image field of view), as well as discrimination between predominant ejecta types (ash, lapilli, bombs or
97 blocks). Between the end of the 2002-03 effusive eruption and the onset of the 2007 eruption, the INGV-CT
98 visual monitoring system was greatly improved with the installation of four additional cameras. These
99 included one visual camera and one thermal infrared camera (SPI) at Il Pizzo, plus one visual camera
100 (SQV400) and one thermal infrared camera (SQT400) at the 400 m elevation. The latter two cameras were
101 located on the eastern flank of SDF ~800 m from the crater terrace. From this location the cameras provided
102 a view of the NE crater and the eastern sector of SDF (Fig. 1c). This location is crucial because the eruptive
103 fissures that opened during the last four effusive episodes (1975, 1985-86, 2002-03 and 2007) breached the
104 NE flank of the crater terrace [*Capaldi et al.,* 1978; *De Fino et al.,* 1988; *Calvari et al.,* 2005a, 2005b;
105 *Marchetti et al.*, 2009] and thus fed activity in this sector. Additionally, on 12 March 2007 while lava effusion
106 was still ongoing, a fifth thermal infrared camera was installed on the eastern margin of the SDF at the 190 m
107 elevation (SCT190, Fig. 1c). From this location the number and position of active lava flows, as well as the
108 development of lava flow field features, could be tracked.
109 Thermal camera SPI is an OPGAL EYE-M320B, and SQT400 is a FLIR ThermoVision® 320M. Both
110 cameras are sensitive across the 8 to 14 μm waveband and have an uncooled microbolometer as the
111 detector. Although they both give 320 x 240 pixel images, which we sample every 2 seconds, SPI has a 60°
112 x 45° field of view (FOV) and SQT400 a 24° x 18° FOV. These correspond to pixel sizes of ~0.2 m over a
113 minimum distance of 250 m (for SPI), and to 1.1 m at a distance of 800 m (for SQT400). The thermal infrared
114 camera installed at the 190 m elevation (SCT190) was a FLIR A40. This gives an inclined view of the SDF
115 and the zone of effusive vents over a mean distance of 300 m. The main difference between the OPGAL
116 camera and the two FLIR cameras is that the OPGAL camera provides just a visual representation of the
117 thermal infrared energy, whereas the FLIR cameras provide radiometric information, i.e., data are calibrated
118 so that temperature information can be extracted for each pixel. All images also record date in the format
119 dd/mm/yy and time in the format hh:mm:ss. All times are given in UTC.
120
121 *2.2. Hand-held thermal imagery*
122
123 Ground-based thermal imaging was first used at Stromboli during a preliminary deployment at Il Pizzo in
124 2001 by *Dehn et al.* [*2001*]. Further deployments proceeded campaign style, with camera's being deployed

for a few days every year between 2001 and 2004 to examine the dynamics of the Strombolian eruptions [*Patrick et al.*, 2007]. With the onset of the 2002-03 effusive eruption, as during the 2007 eruption, thermal surveys were performed daily using a FLIR S65 thermal infrared camera during helicopter flights organised by Protezione Civile Regione Siciliana and Protezione Civile Nazionale. These 2002-03 helicopter-based deployments are described in *Calvari et al.* [2005a, 2005b], *Harris et al.* [2005b] and *Lodato et al.* [2007]. During the 2007 eruption, such helicopter-based surveys occurred on at least a daily basis between 27 February 2007 and 6 May 2007.

Like the permanently installed FLIR thermal infrared cameras, the S65 model used for the helicopter-based surveys consists of an uncooled microbolometer detector array sensitive across the 8 to 14 μm waveband. It has a 18° x 24° lens and provides 320 x 240 pixel images at up to 60 frames per second. The stated precision of the instrument is ±2%, and the thermal sensitivity is <0.08°C at 30°C. The S65 is equipped with an extra filter to detect maximum temperatures up to 1500°C, and can record data in one of three temperature ranges: -40 to 120°C, 0 to 500°C, and 350 to 1500°C. The camera software completes internal calibration and atmospheric correction, so that input emissivity, path length, air temperature and relative humidity allows output of apparent temperatures corrected for emissivity and atmospheric effects. While atmospheric parameters and path length are routinely measured during each thermal survey, we used an emissivity of 0.95, a value which is typical for basalt at Stromboli in the 8 to 14 μm waveband [*Harris and Stevenson*, 1997]. Based on thermal measurements made during effusive eruptions at Etna, as well as on Stromboli during 2002-03, we performed thermal surveys early in the morning to avoid solar heating problems [*Calvari and Pinkerton*, 2004], tried to capture images from the zenith position [*Ball and Pinkerton*, 2006], and repeated the same flight-path every day so as to obtain images that had comparable geometries [*Calvari et al.*, 2005a, 2005b; *Harris et al.*, 2005b]. Corrections resulting from pixel size differences due to varying distances to the target, estimated from the difference between the helicopter location obtained using onboard GPS and locations of known ground-control points, were applied following *Harris et al.* [2005b]. The method of *Harris et al.* [2005b] was also applied to estimate effusion rates from the thermal camera data. Apparent temperatures will still be affected by the presence of aerosols, volcanic gases, and airborne volcanic ash along the path length. This will result in an error in the estimate of true surface temperature [*Calvari et al.*, 2005a, 2005b; *Sawyer and Burton*, 2006; *Spampinato et al.*, 2008b, 2009].

2.3 AVHRR and MODIS satellite thermal data

For satellite-derived effusion rates we have used data from AVHRR and MODIS, two sensors flown on polar orbiting satellites capable of detecting hot spots due to volcanic activity as well as providing data, which can be applied to estimate the area, heat flux and effusion rate of active lava flows [e.g., *Harris et al.*, 1997; *Wright et al.*, 2001; *Hirn et al.*, 2009]. Both detectors have previously been used to provide effusion rates for the 1985-86 and 2002-03 effusive eruptions of Stromboli by *Harris et al.* [2000, 2005b], *Calvari et al.* [2005a, 2005b], *Ripepe et al.* [2005] and *Lodato et al.* [2007]. For effusion rate extraction, all images were examined manually, so that radiances for all pixels identified as being thermally anomalous in images of suitable quality (no cloud cover) were extracted. Extracted radiances were then converted to effusion rate following the methodology of *Harris et al.* [1997] and as applied to AVHRR data for Stromboli by *Harris et al.* [2000] and *Calvari et al.* [2005a, 2005b]. The extraction process results in the generation of an effusion rate range for

each image within which the true, field-measured, value usually lies [see *Harris et al.* 2007b for full review and assessment]. *Dragoni and Tallarico* [2009] have recently reviewed the assumptions underlying the relationship between effusion rate and heat flux, with *Harris and Baloga* [2009] clarifying the methodology and assumptions as applied to low spatial resolution satellite data. Following *Wright et al.* [2001] and *Harris and Baloga* [2009], the extracted value relates to a time-averaged value, not to an instantaneous (effusion rate) value, so that time-averaged discharge rate is likely a better term for the derived value.

3. Explosive activity between the 2002-03 and 2007 effusive eruptions

At the onset of the 2002-03 effusive eruption, the floor of the crater terrace collapsed to leave a ~50 m deep elongate crater. Explosive activity died out at the crater terrace during the first four months of the 2002-03 eruption, with the free-surface and explosive activity recovering as the rate of effusion declined [*Ripepe et al.*, 2005]. As a result, by the end of the 2002-03 effusive eruption (in July 2003) strombolian activity had resumed at the crater terrace. Following the 2002-03 effusive eruption, persistent explosive activity generated spatter, scoria and ash that steadily filled the collapse feature that had formed at the onset of the 2002-03 effusive event. Thus, the elongate crater evolved into a platform on which hornitos and cinder cones developed. To achieve this fill we estimate that an approximate volume of 1.5×10^6 m^3 of material had to have been deposited between July 2003 and February 2007, resulting in a mean fill rate of ~0.01 m^3 s^{-1}. It is worth noting that, as described in previous papers [e.g. *Washington*, 1917; *Calvari et al.*, 2005a, 2005b; *Harris and Ripepe, 2007a*], the position of the active vents has remained almost constant during the last century, even after major morphological changes such as the collapse events of 2002-03 and subsequent refilling by tephra.

The rate of explosive activity, and hence filling of the collapse feature, was not constant with time. To obtain a semi-quantitative description of the eruptive activity during this time, we used the images recorded by camera SPI (which views the entire crater area) to calculate a daily mean for the number of explosions per hour. To do this we simply counted the total number of events observed during each day of cloud-free observation, and divided by 24 hours. Figure 2 shows the pattern of explosive activity from 24 October 2003 until the onset of the 2007 eruption. The period between 17 September 2006 and 21 January 2007 lacks data owing to camera malfunction. A few peaks, when the number of explosions reached 10 to 18 per hour, can be identified between the end of October 2003 and February 2004. After this we observe a stable level, with the number of explosions remaining below 10 per hour from the end of March 2004 until November-December 2004. During January 2005 the average number of explosions increased to between 25 and 30 per hour. Between March 2005 and the onset of the 2007 eruption, a general increasing trend in the number of explosions per hour can be observed. This is punctuated by five peaks in December 2005, January 2006, April 2006 (01/04/06), July 2006 (15/07/06) and 16 February 2007 (16/02/07). The number of explosions increased to a climax of between 25 and 30 explosions per hour twelve days before the start of the 2007 eruption (Fig. 2). These values compare with a typical rate of 8-9 explosions per hour [*Harris and Ripepe*, 2007a; *Ripepe et al.*, 2009].

4. Chronology of the eruption

4.1 Onset of the 2007 effusive activity

Between the end of December 2006 and February 2007, an increase in volcanic tremor was recorded by the Osservatorio Vesuviano (INGV-OV) seismic network. In addition, the frequency of VLP (Very Long Period) seismic events increased, with event locations clustered at ~200 m below the summit craters [*Martini et al.*, 2007], a location typical for Stromboli [*Chouet et al.*, 2003]. In January 2007, the ground-based linear synthetic aperture radar (GB-InSAR), installed on the eastern flank of the SDF, showed a progressive acceleration in the deformation on the NE crater [*Casagli et al.*, 2009]. In addition, tremor, pressure recorded by infrasonic sensors and the number of explosive events per hour began to increase from January onwards [*Ripepe et al.*, 2009]. By the first half of February deformation had spread to also involve the upper portion of the SDF [*Casagli et al.*, 2009].

When the eruption began on 27 February 2007, the deformation rates recorded by the GB-InSAR were higher than the measurement capability of the radar device [*Casagli et al.*, 2009]. At ~9:00 on the same day and about four hours before the start of the onset of effusive activity, the INGV-OV seismic network recorded several signals associated with landslides, sometimes superimposed on the volcanic tremor [*Martini et al.*, 2007]. Landslides continued during the next few hours, and at 12:39 a stronger landslide was recorded [*Martini et al.*, 2007]. An effusive fracture was then observed as opening within the northern rim of the NE crater at 12:49, with the fracture quickly propagating NE [*Marchetti et al.*, 2009]. An air-based thermal survey using the helicopter of Protezione Civile Regione Siciliana was promptly arranged. As a result, the initial effusive phases of the 2007 eruption could be reconstructed from the images recorded by the INGV-CT web-cameras as well as from thermal images collected during the helicopter surveys carried out during the afternoon of 27 February.

Early on 22 February 2007, just before the onset of effusive activity, explosive activity was almost continuous at the NE and Central craters (Fig. 1d), with more than 20 events per hour (Fig. 2). Images recorded by SPI at 10:38 on 27 February, showed an elongate thermal anomaly consistent with the development of a fracture that, after 11:40, propagated gradually NE from vent bN_2 towards bN_1 (Fig. 3a-b). This was accompanied by an increase in the intensity of explosive activity within the SW crater with explosions reaching ~200 m above the vents. The bS_1 vent of the SW crater (Fig. 1d) was a hornito-like structure producing jets of spatter, and vent bS_2 (Fig. 1d) fed ash-rich explosions without incandescent ejecta. Ash emissions from bS_2 always followed explosions from the Central and NE craters. At 12:01 a small portion of the bN_2 hornito collapsed (Fig. 3b).

After ~12:00, explosions at vent bN_1 were persistent and ballistics reached heights up to a few meters, resulting in fast accumulation of spatter around the vent. At 12:23, SQT400 revealed a persistent hot spot on the NE rim of bN_1. This marked the continuation of fracture propagation between bN_2 and bN_1, with the fracture system now extending to the outer rim of the crater terrace. At the same time, a second fracture opened within the NE crater, developing parallel to the previous fracture.

By 12:24 the vent bN2 was emitting a small lava flow. This flow remained confined within the NE crater, ponding in the saddle between vents bN_2 and bN_1 (Fig. 3c). At 12:32, a second hot spot appeared on the NE crater rim marking the intersection of the second fracture with the outer rim of the crater terrace. Analysis of

246 data recorded by camera SPI allowed us to assess the direction of fracture development. The first and
247 northernmost fissure within the NE crater propagated NE (i.e., from bN_2 to bN_1), whereas the southernmost
248 fissure opened later and propagated SW (i.e., from bN_1 to bN_2). Between 12:32 and 12:43, both fractures
249 propagated towards the NE, with propagation being accompanied by explosions, and by gas/steam emission
250 from the NE crater that eventually obscured visibility at SPI.

251 At 12:48, SQT400 captured the opening of a vent (Vent 1, Fig. 1c and Fig. 3d) and the emplacement of a
252 lava flow (Fig. 3e) on the 2002-03 lava shield (Pianoro) located on the upper SDF at ~650 m a.s.l. This fed
253 the first lava flow (FL1, Figs. 3e-i, 4, 5) that was emplaced northwards down the SDF. By 12:59 this had
254 spread across the break in slope at the top of the SDF (Fig. 3f-g) and reached the sea around 13:03, when
255 SQV400 showed a vapour cloud rising above the sea entry (Fig. 3h-i). This means that the flow travelled a
256 distance of 1.2 km (the distance from the vent to the coast) in 15 minutes, so that the mean speed of the flow
257 front was ~1.3 m s^{-1}. This lava flow emplaced on the >30° steep SDF slope, and its velocity was comparable
258 with the 28 December 2002 lava flow reported by *Lodato et al.* [2007]. Lava flow emplacement was
259 accompanied by little landslides that were active on the SDF at any elevation below the summit craters (Fig.
260 4). FL1 was fed at least until 15:00.

261 Explosive activity at bN_1 lasted until 12:56, when activity at this vent died out. At 13:05 the rapidly
262 deposited spatter around bN_1 collapsed to form a small landslide of hot debris, as revealed by SQT400. At
263 12:48 and 13:32, single bursts of hot gas were observed at the base of the eruptive fissure on the Pianoro
264 and then along the NE fissure until 13:25. After 13:32, no more explosive activity occurred either at the
265 summit craters or at the base of the eruptive fissure (~650 m a.s.l.).

266 At 14:57, a new lava flow (FL2, Fig. 4) was erupted from the base of the NE fissure. This initially spread
267 across the Pianoro. At 15:01, this flow descended the steep slopes on the eastern margin of the SDF to
268 reach the sea in just a few minutes, where it generated a second sea entry and associated vapour cloud.
269 With the formation of FL2, supply to FL1 ceased and this flow began to cool.

270 At 15:35 a third lava flow (FL3) appeared in a central position between the two previous flows. This was
271 probably an overflow from the main channel formed along FL2 (Fig. 4). Evidence for this is the fact FL3 had
272 already stopped moving at 15:44. Channel overflows are usually short-lived [e.g., *Bailey et al.*, 2006; *Harris*
273 *et al.*, 2009], so that the short life of this flow appears to support it's origin as an overflow.

274 After 16:00, all three lava flows appeared to be no longer supplied and were cooling. Although
275 incandescent blocks detaching from the margins still exposed the hot inner portions of the cooling flows (Fig.
276 5a-b), a thermal helicopter survey at 16:30 showed FL1 to be cooling and surrounded by landslides. At the
277 same time FL2 was only slowly moving, although the incandescent front of FL3 was visible between dust
278 clouds, and two vapour columns were apparent where flows were entering the sea (Fig. 4). Between 16:00
279 and 18:00, SQT400 showed glow, possibly due to weak explosive activity within the SW crater of the crater
280 terrace. Between 18:00 to 18:36, a small and slow moving lava flow was emplaced over FL3 and FL2, but
281 activity appeared to be waning.

282

283 *4.2 Effusion from the 400 m vent (Vent 2)*

At 18:25:59 on 27 February, a thick ash and vapour column was recorded by SQV400 (Fig. 5a-f). This heralded the opening of a new effusive vent on the SDF at the 400 m elevation (Vent 2, Fig. 1c). The opening of this vent was recorded also by SQT400 that imaged initial explosions from this site immediately followed by the formation of hot debris flows. As also occurred in 2002-03 [*Pioli et al.*, 2008], debris reached the sea within a few minutes, forming a dense vapour cloud that obscured visibility. At 18:25:59, SQV400 recorded the first lava flow (FL4, Fig. 5c-e) erupted from this vent. This flow reached the sea within minutes. After 19:00, vigorous, pulsing, degassing started at Vent 2 (Fig. 1c). This become more vigorous with time. At 20:34:02, SQT400 recorded a sudden gas explosion in the area of Pianoro.

The apparent effusion rate from Vent 2, evaluated on the basis of the glow observed from SQV400, dropped on 28 February after 1:38. This was matched by a decline in the frequency of gas pulses from the same vent. Between 04:00 and 05:00, Vent 2 deepened by a few meters, so that it was no longer visible from SQV400, with this camera just showing the gas cloud released from the vent to be spreading southwards.

On 28 February, a helicopter-based thermal survey at ~08:30 revealed a depression just above Vent 2, and a number of degassing fractures on Pianoro, just at the base of the NE crater (Fig. 6a-b). Vent 2 remained active until the final day of the eruption on 2 April, with lava emitted by Vent 2 accumulating along the shore to significantly modify the coastline, forming a bench that extended seawards by several tens of meters. This bench was particularly prominent in early March.

4.3 Collapses within the crater terrace, 4-9 March

From 4 March, large blocks were seen falling from the crater rim to the crater floor. Onset of rock fall activity could have been earlier, but could not be confirmed due to poor weather conditions which hampered visual and thermal observations. By this time, a field of concentric, arcuate fractures had also opened around the craters. Rock falls became more common in the following days to cause a significant widening of the crater rim and a thick accumulation of debris on the crater floor. At the same time there was a visible widening of the concentric fractures surrounding the craters. Rock falls were mostly concentrated around the NE crater. Images from SPI showed how this rock fall activity modified the profile of the crater rim (Fig. 7a-c), especially at the NE sector (in the foreground of Fig. 7c) whose rim became sufficiently low to allow viewing inside the crater.

A helicopter-based thermal survey on 7 March showed that the fractures were beginning to extend into the craters, following the main (NE-SW) structural trend of the island. The fractures evolved rapidly during the next two days, when large blocks collapsed into the craters to form a thick pile of debris on the crater floor. The volume of material accumulated on the crater floor through collapses was estimated at 1-2 x 10^6 m^3 [*Neri and Lanzafame*, 2009].

Deep explosive activity from below the debris deposit continued to occurr, with rock falls within the craters often accompanied by ash emissions and gas-rich explosions from the vents still active below the

debris carpet. No change was observed in the position of the vents within the crater terrace when compared to the pre-eruptive distribution. The persistence of explosive activity at the crater terrace suggested that magma was still present at a shallow depth below the debris carpet, and that the debris was not causing complete obstruction of the vents. Collapses continued even after the end of the effusive eruption, persisting at least until the end of June 2007.

4.4 Shut down of Vent 2, development of the 550 m elevation vent (Vent 3), and reactivation of Vent 2

Between 7 and 8 March, the output rate from Vent 2 decreased, with effusion from this vent completely shutting down on the afternoon of 8 March. On 9 March a new vent (Vent 3, Figs. 1c and 8a) opened at 550 m a.s.l. on the N flank of the NE crater, in the same position as the 550 m elevation vent of the 2002-03 eruption as mapped by *Calvari et al.* [2005a, 2005b].

A few minutes before 15:00 on 9 March, the Guardia di Finanza Guides reported rock falls, landslides and gas emissions coming from the middle of the SDF, where Vent 3 soon opened to immediately feed lava flow. Analysis of the thermal images recorded by SQT400 allowed us to plot maximum apparent temperature against time for the lower portion of the SDF (Fig. 8b). Although the area covered by the camera did not include the location of Vent 3, which was behind the 2002-03 lava flow field, Figure 8b shows a sudden increase in maximum apparent temperature at 13:31:55, with values of ~300°C. This increase we attribute to the presence of lava fed from Vent 3. Lava reached the sea at 17:43, giving rise to a thick vapour cloud. Vent 3 remained active for less than 24 hours.

While Vent 3 was closing down, effusive activity at Vent 2 renewed. Vent 2 remained active until 2 April, when the eruption ceased in the early afternoon. Vent 3 produced just a narrow lava flow in the middle of the SDF (Figs. 1c and 8a). This lava flow soon disintegrated so that it was no longer visible just a few days after its emplacement. Such crumbling behaviour and volume loss is typical of lava flows emplaced on Stromboli's steep slopes [*Lodato et al.*, 2007]. The steep topography and the loose, fine-grained material that made up the surface at this location accelerated the disintegration of the flow. The location of the flow was also rapidly covered by debris tumbling from sources located higher on the SDF, as was observed during the 2002-03 eruption [*Calvari et al.*, 2005a, 2005b].

4.5 The paroxysm of 15 March

On 15 March, while lava output from Vent 2 was still ongoing, a major, paroxysmal, explosion occurred at 20:38:16 from the crater terrace. The explosion was recorded by the three INGV-CT web-cameras installed on the upper part of the volcano; each offered different views and details of the event (Fig. 9). Camera SPI gave a good overall view of the vents within the crater terrace with a frame rate of 2 seconds (Fig. 9a-d) but, being ~250 m away from the vents, was soon destroyed by fallout from the eruption cloud. However, it showed that the explosion started with small volume collapses from the inner crater rim and emission of a dilute ash cloud (Fig. 9a). Two seconds later a dense, hot cloud of bombs, lapilli and lithics was erupted from

360 the NE crater (Fig. 9b), with a muzzle velocity of ~100 m s^{-1} [*Andronico et al.*, 2007]. This opening sequence
361 of events was very similar to that recorded at the onset of the 5 April 2003 paroxysm at Stromboli [*Calvari et*
362 *al.*, 2006; *Harris et al.*, 2008]. The explosion then propagated across the crater terrace to also involve the SW
363 crater (Fig. 9c-d).

364 The paroxysm, observed from SQT400 (Fig. 9e-h) showed two clouds produced by the two crater
365 regions (N and S; Fig. 9f). These two clouds spread in opposite directions (Fig. 9f-g) to reach heights of well
366 over 500 m above the craters (Fig. 9g-h), i.e., they extended beyond the field of view of our camera which
367 covered a zone 500 m above the craters. A maximum height of 3000-3500 m a.s.l. was estimated from
368 satellite images [*Spinetti et al.*, 2007], which translates to ~2250-2750 m above the craters. Camera SQT400
369 also showed four other similarities with the 5 April 2003 paroxysm as described by *Calvari et al.* [2006], *Rosi*
370 *et al.* [2006] and *Harris et al.* [2008]:

371 (1) The eruption was characterized by multiple explosions from the three summit crater zones,
372 packaged into three distinctive events (Fig. 9h), as revealed by peaks in the maximum apparent
373 temperature record derived from SQT400 thermal images (Fig. 9i).

374 (2) Column collapse fed pyroclastic flows extending up to Bastimento (Fig. 9h).

375 (3) The paroxysm continued for ~7 minutes, with fire fountaining shifting to the SW crater region as
376 the event developed and becoming less intense, with the number and intensity of events
377 gradually decreasing.

378 (4) The paroxysm erupted lithic blocks and juvenile material that reached a lowest elevation of 300
379 m a.s.l. Several hot blocks triggered vegetation fires, and a shower of ash and lapilli covered the
380 villages of Ginostra and Stromboli.

381 The paroxysm caused a further widening of the crater terrace, with a large portion of the South rim being
382 removed by the explosion.

383

384 *4.6. Lava flow activity after 15 March*

385

386 After the 15 March paroxysm, a general decreasing trend was observed in the lava flow output from
387 Vent 2, until 20 March. This decrease was reflected by lava flow bifurcation and the development of many
388 active lobes that often did not reach the sea, as was observed during periods of decreased output at the
389 2002-03 flow field [*Calvari et al.*, 2005a, 2005b; *Lodato et al.*, 2007]. On 20 March, an apparent increase in
390 output was recorded by SQT190, which showed a second lava flow extending down the SDF. An increase in
391 output was also suggested by the fact that the lava flows also began to lengthen to again reach the sea. A
392 further decrease in output in the following days was reflected in the formation of lava tubes in the upper part
393 of the lava flow field, and by piling up of flows above the lava delta that had formed at the coast. Lava tubes
394 progressively extended between 20 and 24 March, with continued decrease in output from Vent 2 causing
395 the lava flow fronts to halt at progressively higher elevations. On 31 March, an increase in output from Vent 2
396 again caused the flow fronts to reach the sea, triggering the formation of thick steam columns. This increase
397 lasted only a few hours, so that by the afternoon of 31 March there was a new regression, with flow fronts

stopping short of the sea. Output decreased again over the following days, with the effusive eruption completely stopping between ~ 9:00 and ~16:00 of 2 April. In fact, three small flows were still active during the helicopter survey carried out at 9:00, whereas just vent incandescence was observed during the next survey carried out at 16:00

5. Effusion rates from thermal data

Effusion rates estimated from helicopter- and satellite-collected data during Stromboli's 2007 were, generally, in good agreement (Table 1 and Fig. 10), with errors typically being ±40%, a value which is comparable to errors affecting field-based measurements [e.g., *Harris and Neri*, 2002; *Calvari et al.*, 2003, 2005a, 2005b; *Lautze et al.*, 2004; *Bailey et al.*, 2006; *Harris et al.*, 2007]. On 4 March, we were able to apply a different approach to extract effusion rates and cross-check the thermal-data-derived values. On this day we could estimate channel dimensions and, by taking images collected at known times and tracking blocks moving on the channel surface, estimate a flow surface velocity of 1.7 m s^{-1}. Hence, using a velocity value that was 2/3 of the surface velocity (as suggested by *Calvari et al.* [2003]), and considering a channel width of 3 m and depth of 1 m, we obtained an effusion rate of ~3 m^3 s^{-1}. This was consistent with both satellite- and FLIR-derived values for the same day (Fig. 10a). Multiple helicopter-based measurements performed on the same day also allowed us to track small fluctuations in effusion rate and check the repeatability of our measurements. On 26 March, for example, we carried out measurements three times: at 7:00, 10:45 and 14:00. These thermal camera data yielded effusion rates of 0.7±0.4, 0.8±0.5, and 0.9±0.5 m^3 s^{-1}, respectively.

5.1. Effusion rate chronology from the thermal image time series

The 2007 eruption was first evident as a major thermal anomaly in AVHRR imagery acquired at 20:06 on 27 February 2007. About an hour later, at 21:00, the first eruption-related thermal anomaly was detected by MODIS. Throughout the effusive event, a total of 219 AVHRR and 118 MODIS images were acquired. Of these, 20 AVHRR and 18 MODIS images had sufficient quality to allow hot spot analysis and conversion to effusion rate. Within the dataset, four periods (spanning 28 February – 4 March, 6 – 11 March, 18 – 25 March, and 2 – 11 April) suffered prolonged cloud cover, so that no images of suitable quality for analysis were available during these periods.

Effusion rates obtained from the FLIR, AVHRR and MODIS data are given in figure 10a and table 1. Data derived from the three data sets show identical trends, with values peaking between 17 and 19 m^3 s^{-1} during 27-28 February (Fig. 10a). This peak was followed by a decline to 1 to 4 m^3 s^{-1} by 4 March. Effusion rates remained at similar, low, levels throughout the remainder of the eruption, with mean values and standard deviations during the cloud-free periods of 2.0±1.2 m^3 s^{-1} (4 – 6 March, 6 images), 1.4±1.4 m^3 s^{-1} (11 – 17 March, 17 images), 1.2±1.0 m^3 s^{-1} (26 – 29 March, 10 images), and 1.2±0.9 m^3 s^{-1} (31 March – 1 April, 6 images). Thus, except for the short effusion rate peak at the onset of the eruption, activity was characterised by a dominant phase of low effusion rates. However, as observed during previous effusive eruptions at Stromboli [*Harris et al.*, 2005b; *Lodato et al.*, 2007] and Etna [*Lautze et al.*, 2004; *Harris et al.*, 2005a; *Bailey et al.*, 2006; *James et al.*, 2007], even apparently steady, low effusion rate eruptions undergo variations over

time scales of minutes-to-hours. During the 2007 eruption for example, the generally steady effusion rate trend recorded between 11 and 17 March showed variations ranging between 5.0 and 0.2 $m^3 s^{-1}$ (Fig. 10a) and displayed three effusion rate cycles. Each cycle was characterised by a relatively high effusion rate phase followed by a low effusion rate phase. The first cycle began with a maximum of 5.3 $m^3 s^{-1}$, as recorded on 11 March. This was followed by a decrease to 0.5 $m^3 s^{-1}$ by 12 March (Table 1). The onset of the second cycle was marked by a recovery to 4.7 $m^3 s^{-1}$ by 21:00 on 13 March. Effusion rates declined again to 0.6 $m^3 s^{-1}$ by 00:58 on 15 March. The last cycle began with an increase to 5.0 $m^3 s^{-1}$ (observed at 12:24 on 16 March) followed by a final decrease. Such lava effusion rate cycles were also observed during the 2002-03 effusive eruption at Stromboli by *Harris et al.* [2005b] and were ascribed to recovery of the magma level in the central column during low effusion rate periods. Such recovery will increase the hydrostatic head in the conduit. An increase in the hydrostatic head then results in an increase in the effusion rate from the dike tapping the conduit at a lower level, which then results in drainage of the shallow system so that the cycle begins anew.

Integration of effusion rates over time yielded cumulative volumes (Fig. 10b) and gave a final erupted volume of between 3.2 x 10^6 and 11 x 10^6 m^3. The mean volume of 7.1 x 10^6 m^3, when erupted over 34 days, gives a mean output rate of 2.4 $m^3 s^{-1}$. This is an order of magnitude higher than the mean output rates calculated during Stromboli's 2002-03 eruption (0.32±0.28 $m^3 s^{-1}$, *Lodato et al.*, 2007) and 1985-86 eruption (0.34±0.05 $m^3 s^{-1}$, *Harris et al.*, 2000). The cumulative volume plot of figure 10b reveals the decline in effusion rate after the first 5.5 days from an inflexion between 28 February and 4 March. As a result, we move from a period of a high rate of volumetric increase (6.6 x 10^5 $m^3 d^{-1}$) during the first 5.5 days of the eruption to a low rate of increase (1.2 x 10^5 $m^3 d^{-1}$) thereafter. This means that 51% of the total volume was erupted over the first 5.5 days, or 16% of the eruption by time.

5. Discussion

As was observed prior to the 2002-03 eruption [*Calvari et al.*, 2005a, 2005b; *Burton et al.*, 2008], explosive activity at the crater terrace increased to relatively high levels prior to the onset of Stromboli's 2007 effusive eruption. *Calvari et al.* [2005a, 2005b], *Burton et al.* [2008] and *Ripepe et al.* [2009] have argued that the number of explosions per hour is an indirect measure of magma input rate and magma level within the conduit, where an increasing magma level can be associated with more violent and frequent explosive activity. Hence, we interpret the increase in the number of explosions per hour prior to the 2007 effusive eruption as being a result of an increase in the level of the magma free-surface within the conduit. This is consistent with other geophysical (seismic and infrasonic) data which showed explosion rate, pressure and tremor increasing after January 2007 [*Giudicepietro et al.,* 2009; *Ripepe et al.*, 2009]. This increase was interpreted by *Ripepe et al.* [2009] as evidence for increased magma supply to the shallow system. The main phases of the 2007 eruption are sketched in figure 11. The intense explosive activity and increased magmastatic pressure within the conduits promoted the breaching of the conduit system and extension of a dike to the NE [*Marchetti et al.*, 2009; *Neri and Lanzafame*, 2009]. The observed SW-NE propagation direction of the dike is consistent with our thermal camera based observations of the shifting location and style of activity within the crater terrace, where hot fractures and activity were observed to propagate to the NE in the hours prior to the onset of effusion (Fig. 11a-b). Dikes extending from the central conduit fed effusive vents in the same location during the 1985-86 and 2002-03 eruptions [*De Fino et al.*, 1988; *Calvari*

480 *et al.*, 2005a, 2005b]. Thus, the NE flank of the crater terrace currently appears prone to failure during times
481 of increased activity and magmastatic pressure.
482 In addition to the propagation direction of the eruptive fissure and location of the initial effusive vent, a
483 number of other similarities were observed between the opening phases of the 2002-03 and 2007 effusive
484 eruptions. For example, as in 2002-03, opening of effusive vents were heralded by landslides spreading
485 along the SDF. These formed the dust clouds apparent in figures 3, 4 and 5. These landslides were also
486 detected by the INGV-OV seismic network [*Martini et al.,* 2007] and can be considered among the precursors
487 to effusive activity and the opening of effusive vents at Stromboli. Effusion then typically begins with a short,
488 high effusion rate peak as the central conduit is tapped, followed by a longer waning period over which small
489 variations in effusion can be observed. As previously discussed for Stromboli by *Lodato et al.* [2007] and
490 *Harris et al.* [2005b], both the long and short time scales of variation have implications for the magma
491 dynamics of the shallow system. For example, following *Wadge* [1981] the short waxing and long waning
492 phase observed in the effusion rate trend can be interpreted as tapping of a pressurized source. However,
493 the effusion rate variations were not smooth, where the front of FL3 showed pulsating movements and
494 stopped a short time before the opening of Vent 2 (Fig. 5a-b). We interpret this behaviour as the result of
495 small variations of magma level within the feeder dike during its propagation to force short-term variations in
496 the effusion rate from that dike (Fig. 11c-d).
497 As during 2002-03, high effusion rates at the onset of the eruption led to rapid drainage of the shallow
498 system and triggered summit collapses. Collapses propagated to NE along the feeder dike, causing
499 blockage of Vent 2, which stopped erupting on the afternoon of 8 March (Fig. 11e). This probably caused an
500 accumulation of magma and overpressure in the upper conduit, resulting in the opening of a new vent (Vent
501 3) at the 550 m elevation on the following day (Figs. 8, 11e). The position of Vent 3 was very close to the
502 conduit, where a similar sequence of vent opening was observed at the onset of the 2002-03 effusive
503 eruption [Calvari et al., 2005a, 2005b]. The blockage in the feeder dike must have been removed quite
504 quickly, because Vent 3 erupted for less than 24 hours, with activity at Vent 2 resuming on the following day
505 and lasting until the end of the eruption (Fig. 11f).
506 But why was the main active vent during 2007 as low as 400 m a.s.l., whereas in 1975, 1985-86 and
507 2002-03 the main active vent was located at 500-550, 650, or 670 m a.s.l.? We believe that there is a simple
508 explanation for this. The 2002-03 eruption had began with small volume flank failures which left a collapse
509 scar in the SDF [*Bonaccorso et al.*, 2003]. The eastern margin of the SDF continued a sliding movement
510 after the 2002-03 eruption [*Tommasi et al.*, 2005; 2008; *Bonforte et al.*, 2008], with a greater displacement in
511 the upper part of the SDF and smaller velocities at the lowest benchmarks [*Bonforte et al.*, 2008]. This likely
512 resulted from the formation of a sliding block whose south-eastern margin was used by the intrusion of the
513 2007 dike (Fig. 12a-b). We thus suggest that the 2007 dike opened along the sliding surface (marked by the
514 yellow dotted line in Fig. 11d-f, and by the green dotted line in Fig. 12b), and that both Vents 2 and 3 formed
515 at the intersection between the topographic slope and the eastern and western margins of the sliding block,
516 respectively (Figs. 11d-f, 12b).
517 Effusion rates were higher than during the 2002-03 effusive eruption, as seen from the mean output rates
518 which were 0.32±0.28 $m^3 s^{-1}$ during the 2002-03 eruption [*Lodato et al.*, 2007] as opposed to ~2.4 $m^3 s^{-1}$
519 during the 2007 eruption. The lower elevation of the main effusive vent during the 2007 eruption, i.e. 400 m
520 a.s.l. in 2007, compared with 550-670 m during 2002-03, may have caused the higher effusion rates during

2007. The increased hydrostatic head resulting from a lower vent elevation in 2007 may, for example, have resulted in higher effusion rates during initial tapping and drainage of the shallow system. Conduit drainage may, in turn, have been responsible for de-pressurisation of the system facilitating up-rise of gas-rich magma to cause the 15 March paroxysm. Such de-pressurisation is consistent with ground deformation data that was revealed by continuous deflation during the entire 2007 eruption [*Bonaccorso et al.*, 2009].

The 15 March 2007 paroxysm itself was very similar to that of 5 April 2003. The main similarities are as follows:

(i) Both paroxysms occurred after a phase of no explosive activity at the summit craters due to conduit emptying during an effusive eruption.

(ii) Both began with a short phase of lithic ash emission.

(iii) During both paroxysms explosive activity propagated from the NE crater to the SW crater with time.

(iv) Both events involved the eruption of lithics, high-porphyric scoria, and low-porphyric pumice [*Bertagnini et al.*, 1999; *Francalanci et al.*, 2008; *Landi et al.*, 2009].

(v) Both events had similar durations, with the 5 April 2003 event lasting 6-9 minutes [*Calvari et al.*, 2006; *Harris et al.*, 2008], and the 15 March 2007 event ~7 minutes.

(vi) Both events comprised several eruptive pulses.

However, the 15 March 2007 event was characterised by fire fountaining that formed distinct columns over each of the three crater zones, as was well visible from the SQT400 camera (Fig. 9). In comparison thermal and digital camera data for the 5 April 2003 paroxysm revealed pulsating ash columns [*Calvari et al.*, 2006]. Also, prior to the 5 April 2003 paroxysm *Calvari et al.* [2006] recorded an increase in maximum apparent temperature within the crater terrace. No significant increase in the maximum apparent temperature was detected within the crater terrace before the paroxysm of 2007. However, distance and viewing angle may be significant factors in preventing detection of subtle temperature variations within the crater terrace, especially when considering data from cameras that do not have a view into the craters, as is the case for camera SQT400.

6. Concluding remarks

The 2007 effusive eruption of Stromboli showed similar features to those observed during the previous effusive event of 2002-03. Both eruptions began after a precursory phase of increasing explosive activity, and were heralded by a peak in the number of explosions per hour at the summit craters. Both eruptions began with the opening of an eruptive fissure on NE flank of the crater terrace, and both involved paroxysms that occurred during lava effusion. However, some important differences were observed in 2007. These were:

1 The opening of two parallel fissures on the NE flank of the crater terrace;

2 The lower elevation (400 m) of the main effusive vent;

3 The higher mean output rate in 2007, which was an order of magnitude higher than those of the two previous eruptions (1985-86 and 2002-03).

We suggest that these differences were influenced by the structural dynamics of SDF, which had been sliding between the 2002-03 and 2007 eruptions [*Tommasi et al.*, 2005; 2008; *Bonforte et al.*, 2008]. Opening of Vents 1, 2, and 3 occurred at the intersection between the SDF slope and the upper, eastern and

562 western margins of the sliding block, respectively. In addition, the lower elevation of the 2007 main effusive
563 vent likely caused faster drainage and depressurisation of the shallow system, and facilitated uprise of the
564 batch of magma that caused the March 2007 paroxysmal event.
565
566
567 **Acknowledgements**
568 We wish to thank S. Cocina of the Protezione Civile Regionale Siciliana for promptly making available the
569 helicopter for the thermal surveys, the pilot G. Maurici and his team for the many flights carried out during the
570 initial phases of the eruption in harsh and difficult conditions; G. Bertolaso and the Protezione Civile
571 Nazionale for their assistance and support during the whole eruption, and the helicopter pilots C. Geri, C.
572 Cullurà, S. Princiotta, E. Zanetti, L. Laudadio and L. Zanazzo. Special thanks to our INGV colleagues from
573 sezione di Catania, Napoli, Palermo, Pisa, Roma and Milano who helped during data collection during the
574 eruption, and especially to G. Lanzafame and M. Neri for the fruitful discussions on the mechanisms of
575 opening of eruptive fissures, and to M. Neri for making Fig. 1. We wish to thank the former Director of INGV
576 sezione di Catania A. Bonaccorso for his continuous encouragement and support to our activities. This work
577 has been possible thanks to the installation and maintenance of the INGV-CT web-camera network carried
578 out by E. Pecora, E. Biale, D. Condarelli, and D. Reitano. This paper was partially supported by a grant to S.
579 Calvari (Project INGV-DPC Paroxysm V2/03, 2008-2010) funded by the Istituto Nazionale di Geofisica e
580 Vulcanologia and by the Italian Civil Protection. Satellite-based effusion rate work by A. Steffke and A. Harris
581 was supported by NASA grant NNG04GO64G "New Tools for Advanced Hot Spot Tracking". The authors
582 wish to thank the reviews by M. James, M. Patrick, R. Arculus, and L. Glaze for their many suggestions that
583 greatly improved the paper.
584
585 **References**
586 Andronico, D., A. Cristaldi, and J. Taddeucci (2007), Eruzione Stromboli 2007: evento parossistico del 15
587 marzo. *INGV-CT report*, Prot. Int. UFVG2007/116, 1-7.
588 Bailey, J.E., A.J.L. Harris, J. Dehn, S. Calvari, S.K. Rowland (2006), The changing morphology of an open
589 lava channel on Mt. Etna, *Bull. Volc.*, DOI 10.1007/s00445-005-0025-6, *68*, 6, 497-515.
590 Ball, M., and H. Pinkerton, (2006), Factors affecting the accuracy of thermal imaging cameras in volcanology.
591 *J. Geophys. Res., 111*, B11203, doi:10.1029/2005JB003829.
592 Barberi, F., M. Rosi, and A. Sodi (1993), Volcanic hazard assessment at Stromboli based on review of
593 historical data, *Acta Vulc.*, *3*, 173-187.
594 Barberi, F., L. Civetta, M. Rosi, and R. Scandone (2009), Chronology of the 2007 eruption of Stromboli and
595 the activity of the Scientific Synthesis Group, *J. Volc. Geoth. Res., 182*, 123-130.
596 Bertagnini, A., M. Coltelli, P. Landi, M. Pompilio, and M. Rosi (1999), Violent explosions yield new insights
597 into dynamics of Stromboli volcano, *Eos, Am. Geoph. Union Trans., 80* (52), 633-636.
598 Bonaccorso, A., S. Calvari, G. Garfì, L. Lodato, and D. Patané (2003), December 2002 flank failure and
599 tsunami at Stromboli volcano inferred by volcanological and geophysical observations. *Geophys. Res.*
600 *Lett.*, *30*(18), 1941-1944.

601 Bonaccorso, A., A. Bonforte, S. Gambino, M. Mattia, F. Guglielmino, G. Puglisi, and E. Boschi (2009), Insight
602 on recent Stromboli eruption inferred from terrestrial and satellite ground deformation measurements,
603 *J. Volc. Geoth. Res.*, doi: 10.1016/j.jvolgeores.2009.01.007.
604 Bonforte, A., M. Aloisi, G. Antonello, N. Casagli, J. Fortuny-Guash, L. Guerri, G. Nunnari, G. Puglisi, A.
605 Spata, and D. Tarchi (2008), Movements of the Sciara del Fuoco, in *The Stromboli Volcano: An*
606 *integrated study of the 2002-2003 Eruption*, edited by S. Calvari, S. Inguaggiato, G. Puglisi, M. Ripepe
607 and M. Rosi, *AGU Geophysical Monograph Series, 182*, 183-200.
608 Burton, M.R., S. Calvari, Spampinato L., Lodato L., Pino N.A., Marchetti E., and Murè F. (2008), Volcanic
609 and seismic activity at Stromboli preceding the 2002-03 eruption, in *The Stromboli Volcano: An*
610 *integrated study of the 2002-2003 Eruption*, edited by S. Calvari, S. Inguaggiato, G. Puglisi, M. Ripepe
611 and M. Rosi, *AGU Geophysical Monograph Series, 182*, 93-104.
612 Calvari, S., and H. Pinkerton (1998), Formation of lava tubes and extensive flow field during the 1991-93
613 eruption of Mount Etna, *J. Geophys. Res., 103,* B11, 27291-27302.
614 Calvari, S., and H. Pinkerton (2004), Birth, growth and morphologic evolution of the "Laghetto" cinder cone
615 during the 2001 Etna eruption. *J. Volc. Geoth. Res.*, *132*, 225-239, doi:10.1016/S0377-0273(03)00347-
616 0.
617 Calvari, S., M. Neri, and H. Pinkerton (2003), Effusion rate estimations during the 1999 summit eruption on
618 Mt. Etna, and growth of two distinct lava flow fields. *J. Volc. Geoth. Res.*, *119*, 107-123, S0377-
619 0273(02)00308-6, ISSN0377-0273.
620 Calvari, S., L. Spampinato, and L. Lodato (2006), The 5 April 2003 vulcanian paroxysmal explosion at
621 Stromboli volcano (Italy) from field observations and thermal data. *J. Volc. Geoth. Res.*, *149*, 160-175,
622 doi:10.1016/j.jvolgeores.2005.06.006.
623 Calvari, S., L. Spampinato, L. Lodato, A.J.L. Harris, M.R. Patrick, J. Dehn, M.R. Burton, and D. Andronico
624 (2005a), Chronology and complex volcanic processes during the 2002--2003 flank eruption at
625 Stromboli volcano (Italy) reconstructed from direct observations and surveys with a handheld thermal
626 camera. *J. Geophys. Res.*, *110*, B02201, doi:10.1029/2004JB003129.
627 Calvari, S., L. Spampinato, L. Lodato, A.J.L. Harris, M.R. Patrick, J. Dehn, M.R. Burton, and D. Andronico
628 (2005b), Correction to “Chronology and complex volcanic processes during the 2002--2003 flank
629 eruption at Stromboli volcano (Italy) reconstructed from direct observations and surveys with a
630 handheld thermal camera”. *J. Geophys. Res.*, *110*, B02201, doi:10.1029/2005JB003723.
631 Capaldi, G., I. Guerra, A. Lo Bascio, G. Luongo, R. Pece, A. Rapolla, R. Scarpa, E. Del Pezzo, M. Martini,
632 M.R. Ghiara, L. Lirer, R. Munno, and L. La Volpe (1978), Stromboli and its 1975 Eruption, *Bull. Volc.*,
633 *41* (3), 259-285.
634 Casagli, N., A. Tibaldi, A. Merri, C. Del Ventisette, T. Apuani, L. Guerri, J. Fortuny-Guasch, and D. Tarchi
635 (2009), Deformation of Stromboli Volcano (Italy) during the 2007 crisis by radar interferometry,
636 numerical modeling and field structural data, *J. Volc. Geoth. Res.*, *182*, 182-200.
637 Chouet, B., P. Dawson, T. Ohminato, M. Martini, G. Saccorotti, F. Giudicepietro, G. De Luca, G. Milana, and
638 R. Scarpa (2003), Source mechanisms of explosions at Stromboli Volcano, Italy, determined from
639 moment-tensor inversions of very-long-period data, *J. Geoph. Res.*, *108*, B1, 2019,
640 doi:10.1029/2002JB001919.

De Fino, M., L. La Volpe, S. Falsaperla, G. Frazzetta, G. Neri, L. Francalanci, M. Rosi, and A. Sbrana (1988), The Stromboli eruption of December 6, 1985 - April 25, 1986: volcanological, petrological and seismological data, *Rend. Soc. It. Min. Petr., 43*, 1021-1038.

Dehn, J., Harris, A., and M. Ripepe (2001), Infrared Imaging of Strombolian Eruptions, *Annual American Geophysical Union Meeting*, San Francisco, CA, USA, December 10-14, 2001.

Dragoni, M., and A. Tallarico (2009), Assumptions in the evaluation of lava effusion rates from heat radiation, *Geophys. Res. Letters*, *36*, L08302, doi:10.1029/2009GL037411.

Francalanci, L., A. Bertagnini, N. Métrich, A. Renzulli, R. Vannucci, P. Landi, S. Del Moro, M. Menna, C.M. Petrone, and I. Nardini (2008), Mineralogical, Geochemical, and Isotopic Characteristics of the Ejecta From the 5 April 2003 Paroxysm at Stromboli, Italy: Inferences on the Preeruptive Magma Dynamics, in *The Stromboli Volcano: An integrated study of the 2002-2003 Eruption*, edited by S. Calvari, S. Inguaggiato, G. Puglisi, M. Ripepe and M. Rosi, *AGU Geophysical Monograph Series, 182*, 331-346.

Giudicepietro, F., L. D'Auria, M. Martini, T. Caputo, R. Peluso, W. De Cesare, M. Orazi, and G. Scarpato (2009), Changes in the VLP seismic source during the 2007 Stromboli eruption, *J. Volc. Geoth. Res.*, *182*, 162-171.

Harris, A.J.L., J.E. Bailey, S. Calvari, and J. Dehn, (2005a), Heat loss measured at a lava channel and its implications for down-channel cooling and rheology, *Geol. Soc. Am. Spec. Paper, 396*, 125-146.

Harris, A.J.L., and S.M. Baloga (2009), Lava discharge rates from satellite-measured heat flux, *Geophys. Res. Letters, 36,* L19302, doi:10.1029/2009GL039717.

Harris, A.J.L., A.L. Butterworth, R.W. Carlton, I. Downey, P. Miller, P. Navarro, and D.A. Rothery (1997), Low-cost volcano surveillance from space: case studies from Etna, Krafla, Cerro Negro, Fogo, Lascar and Erebus, *Bull. Volc.*, *59*, 49-64.

Harris, A.J.L., J. Dehn, and S. Calvari (2007), Lava Effusion Rate Definition, Measurement and Operational Requirements: A Review, *Bull. Volc.*, *70*, 1-22, doi:10.1007/s00445-007-0120-y.

Harris, A.J.L., J. Dehn, M. Patrick, S. Calvari, M. Ripepe, and L. Lodato (2005b), Lava effusion rates from hand-held thermal infrared imagery: an example from the June 2003 effusive activity at Stromboli, *Bull. Volc.*, *68*, 107-117, doi: 10.1007/s00445-005-0425-7.

Harris, A.J.L., M. Favalli, F. Mazzarini, and C.W. Hamilton (2009), Construction Dynamics of a Lava Channel, *Bull. Volc.*, *71*, 459–474, doi: 10.1007/s00445-008-0238-6.

Harris, A.J.L., and M. Neri (2002), Volumetric observations during paroxysmal eruptions at Mount Etna: pressurized drainage of a shallow chamber or pulsed supply? *J. Volc. Geoth. Res.*, *116*, 79-95.

Harris, A.J.L., J.B. Murray, S.E. Aries, M.A. Davies, L.P. Flynn, M.J. Wooster, R. Wright, and D.A. Rothery (2000), Effusion rate trends at Etna and Krafla and their implications for eruptive mechanisms, *J. Volc. Geoth. Res.,* 102, 237-270.

Harris, A.J.L., and M. Ripepe (2007a), Synergy of multiple geophysical approaches to unravel explosive eruption conduit and source dynamics – A case study from Stromboli. *Chemie der Erde*, *67*, 1-35.

Harris, A.J.L., and M. Ripepe (2007b), Temperature and dynamics of degassing at Stromboli. *J. Geophys. Res., 112*, B03205, doi:10.1029/2006JB004393.

Harris, A.J.L., M. Ripepe, S. Calvari, L. Lodato, and L. Spampinato (2008), The 5 April 2003 Explosion of Stromboli: Timing of Eruption Dynamics Using Thermal Data, in *The Stromboli Volcano: An integrated*

study of the 2002-2003 Eruption, edited by S. Calvari, S. Inguaggiato, G. Puglisi, M. Ripepe and M. Rosi, *AGU Geophysical Monograph Series, 182*, 305-316.

Harris, A.J.L., and S.K. Rowland (2009), Effusion rate controls on lava flow length and the role of heat loss: A review, in *Studies in Volcanology: The Legacy of George Walker*, edited by T. Thordarson, S. Self, G. Larsen, S.K. Rowland, and A. Hoskuldsson, *Special Publications of IAVCEI*, *2*, 33–51.

Harris, A.J.L., and D.S. Stevenson (1997), Thermal observations of degassing open conduits and fumaroles at Stromboli and Vulcano using remotely sensed data. *J. Volcanol. Geothem. Res.*, *76*, 175-198.

Hirn, B., C. Di Bartola, and F. Ferrucci (2009), Combined use of SEVIRI and MODIS for detecting, measuring, and monitoring active lava flows at erupting volcanoes, *IEEE Trans. Geosci. Remote Sensing*, doi: 10.1109/TGRS.2009.2014224.

James, M., H. Pinkerton, and S. Robson (2007), Image-based measurement of flux variation in distal regions of active lava flows. *Geochem., Geophys., Geosyst., 8,* Q03006, doi:10.1029/2006GC001448.

Kilburn, C.R.J. (1993), Lava crust, aa flow lengthening and the pahoehoe-aa transition, in *Active lavas: monitoring and modelling*, edited by C.R.J. Kilburn and G. Luongo, *UCL Press, London,* 263-279.

Landi, P., R.A. Corsaro, L. Francalanci, L. Civetta, L. Miraglia, M. Pompilio, and R. Tesoro (2009), Magma dynamics during the 2007 Stromboli eruption (Aeolian Islands, Italy): Mineralogical, geochemical and isotopic data, *J. Volc. Geoth. Res.*, doi:10.1016/j.jvolgeores.2008.11.010.

Lautze, N.C., A.J.L. Harris, J.E. Bailey, M. Ripepe, S. Calvari, J. Dehn, S. Rowland, and K. Evans-Jones (2004), Pulsed lava effusion at Mount Etna during 2001, *J. Volc. Geoth. Res., 137*, 231-246, doi:10.1016/j.jvolgeores.2004.05.018.

Lodato, L., L. Spampinato, A.J.L. Harris, S. Calvari, J. Dehn, and M. Patrick (2007), The Morphology and Evolution of the Stromboli 2002-03 Lava Flow Field: An Example of Basaltic Flow Field Emplaced on a Steep Slope, *Bull. Volc.*, *69*, 661-679, doi:10.1007/s00445-006-0101-6.

Marchetti, E., R. Genco, and R. Ripepe (2009), Ground deformation and seismicity related to the propagation and drainage of the dyke feeding system during the 2007 effusive eruption at Stromboli volcano (Italy), *J. Volc. Geoth. Res., 182*, 155-161.

Martini, M., F. Giudicepietro, L. D'Auria, A.M. Esposito, T. Caputo, R. Curciotti, W. De Cesare, M. Orazi, G. Scarpato, A. Caputo, R. Peluso, P. Ricciolino, A.T. Linde, and S. Sacks (2007), Seismological monitoring of the February 2007 effusive eruption of the Stromboli volcano, *Ann. Gephys.*, *50*, 6, 775-788.

Neri, M., and G. Lanzafame (2009), Structural features of the 2007 Stromboli eruption, *J. Volc. Geoth. Res.*, *182*, 137-144, doi:10.1016/j.jvolgeores.2008.07.021.

Patrick, M.R. (2007), Dynamics of strombolian ash plumes from thermal video: Motion, morphology, and air entrainment, *J. Geophys. Res.*, *112*, B06202, doi:10.1029/2006JB004387.

Patrick, M.R., A.J.L. Harris, M. Ripepe, J. Dehn, D.A. Rothery, and S. Calvari (2007), Strombolian explosive styles and source conditions: insights from thermal (FLIR) video, *Bull. Volc.*, *69*, 769-784, doi: 10.1007/s00445-006-0107-0.

Pioli, L., M. Rosi, S. Calvari, L. Spampinato, A. Renzulli, and A. Di Roberto (2008), The eruptive activity of 28 and 29 December 2002, in *The Stromboli Volcano: An integrated study of the 2002-2003 Eruption*, edited by S. Calvari, S. Inguaggiato, G. Puglisi, M. Ripepe and M. Rosi, *AGU Geophysical Monograph Series, 182*, 105-116.

722 Ripepe, M., D. Delle Donne, G. Lacanna, E. Marchetti, and G. Ulivieri (2009), The onset of the 2007
723 Stromboli effusive eruption recorded by an integrated geophysical network, *J. Volc. Geoth. Res.*, *182*,
724 131-136.
725 Ripepe, M., E. Marchetti, G. Ulivieri, A.J.L. Harris, J. Dehn, M.R. Burton, T. Caltabiano, and G.G. Salerno,
726 (2005), Effusive to explosive transition during the 2003 eruption of Stromboli volcano, *Geology*, *33*, 5,
727 341-344.
728 Rosi, M., A. Bertagnini, A.J.L. Harris, L. Pioli, M. Pistolesi, and M. Ripepe, (2006), A case history of
729 paroxysmal explosion at Stromboli: Timing and dynamics of the April 5, 2003 event, *Earth Plan. Sci.*
730 *Letters*, *243*, 594-606.
731 Rowland, S.K., A.J.L. Harris, M.J. Wooster, F. Amelung, H. Garbeil, L. Wilson, and P. Mouginis-Mark (2003),
732 Volumetric characteristics of lava flows from interferometric radar and multispectral satellite data: the
733 1995 Fernandina and 1998 Cerro Azul eruptions in the western Galàpagos, *Bull. Volc.*, *65*, 311-330.
734 Sawyer, G.M., and M.R. Burton, (2006), Effects of a volcanic plume on thermal imaging data, *Geophys. Res.*
735 *Lett.*, *33*, L14311, doi:10.1029/2005GL025320.
736 Scandone, R., F. Barberi, and M. Rosi (2009), The 2007 eruption of Stromboli: Preface, *J. Volc. Geoth. Res.*,
737 *182*, v.
738 Spampinato, L., S. Calvari, A.J.L. Harris, and J. Dehn (2008a), Evolution of the lava flow field, in *The*
739 *Stromboli Volcano: An integrated study of the 2002-2003 Eruption*, edited by S. Calvari, S.
740 Inguaggiato, G. Puglisi, M. Ripepe and M. Rosi, *AGU Geophysical Monograph Series, 182*, 201-212.
741 Spampinato, L., S. Calvari, C. Oppenheimer, and L. Lodato (2008b), Shallow magma transport for the 2002-
742 03 Mt. Etna eruption inferred from thermal infrared surveys, *J. Volc. Geoth. Res.*, *177*, 301-312,
743 doi:10.1016/j.jvolgeores.2008.05.013.
744 Spampinato, L., S. Calvari, C. Oppenheimer, L. Lodato, and E. Boschi (2009), Revisiting the use of infrared
745 thermal cameras for the surveillance of active volcanoes. *Earth-Sci. Rev.*, in review.
746 Spinetti, C., M.F. Buongiorno, F. Doumaz, M. Musacchio, V. Lombardo, A.J.L. Harris, A. Steffke, and S.
747 Amici (2007), Rapporto eruzione Stromboli 9-16 marzo 2007, pp. 1-9,
748 *http://www.ct.ingv.it/Report/BollettinoCNT_160307_Stromboli%20(2).pdf*
749 Tinti, S., A. Manucci, G. Pagnoni, A. Armigliato, and F. Zaniboni (2005), The 30 December 2002 landslide-
750 induced tsunamis in Stromboli: sequence of the events reconstructed from the eyewitnesses accounts,
751 *Nat. Haz. Earth Sys. Sci.*, *5*, 763-775.
752 Tommasi, P., P. Baldi, F.L. Chiocci, M. Coltelli, M. Marsella, M. Pompilio, and C. Romagnoli (2005), The
753 Landslide Sequence Induced by the 2002 Eruption at Stromboli Volcano, in *Landslide - Risk analysis*
754 *and sustainable disaster management*, edited by K. Sassa, H. Fukuoka, F.W. Wang, and G. Wang,
755 *Springer Verlag, Berlin*, pp. 251-258.
756 Tommasi, P., P. Baldi, F.L. Chiocci, M. Coltelli, M. Marsella, and C. Romagnoli (2008), Slope failures
757 induced by the December 2002 eruption at Stromboli volcano, in *The Stromboli Volcano: An integrated*
758 *study of the 2002-2003 Eruption*, edited by S. Calvari, S. Inguaggiato, G. Puglisi, M. Ripepe and M.
759 Rosi, *AGU Geophysical Monograph Series, 182*, 129-145.
760 Washington, H.S. (1917), Persistence of vents at Stromboli and its bearing on volcanic mechanism, *Geol.*
761 *Soc. Am. Bull.*, *28*, 249-278.

762 Wadge, G. (1981), The variation of magma discharge during basaltic eruptions, *J. Volc. Geoth. Res.*, *11*,
763 139-168.
764 Wright, R., S. Blake, A.J.L. Harris, and D.A. Rothery (2001), A simple explanation for the space-based
765 calculation of lava eruption rates, *Earth Plan. Sci. Letters*, *192*, 223-233.
766 Zanon, V., M. Neri, and E. Pecora (2009), Interpretation of data from the monitoring thermal camera of
767 Stromboli volcano (Aeolian Islands, Italy), *Geol. Mag.*, *146* (4), 591-601.
768
769
770 **Figure Captions**
771
772 **Figure 1 -** (a): Location of the Aeolian Volcanic Arc (AVA) and Stromboli. (b): Island of Stromboli with the
773 outline of the Sciara del Fuoco (SDF) marked by the blue line. The area enlarged in (c) is also located. (c):
774 The 2007 lava flow field (in red) with the feeding vents (in yellow) and location of the INGV-CT web-cameras:
775 SPI (Stromboli Infrared thermal camera at Il Pizzo), SQT400 (Stromboli infrared Thermal camera at 400 m
776 elevation), SQV400 (Stromboli Visible camera at 400 m elevation), and SCT190 (Stromboli infrared Thermal
777 camera at 190 m elevation). CR1 and CR3 mark the South-West and North-East craters. (d): The position of
778 the active vents within the crater terrace as could be seen from the SPI camera located at Il Pizzo, where S,
779 C and N mark the SW, Central and NE craters, within which bS_2, bS_1, bC, bN_2, and bN_1 locate the active
780 vents within each crater as of February 2007. Images (a) to (c) are courtesy of M. Neri [modified after *Neri*
781 *and Lanzafame*, 2009].
782
783 **Figure 2** – Graph showing the daily average frequency of explosions per hour at the crater terrace between
784 24 October 2003 and 27 February 2007, reconstructed using images recorded camera SPI (see figure 1c for
785 camera location).
786
787 **Figure 3 –** Images taken from camera SPI (a-c), SQT400 (d-f) and SQV400 (g-i) (see Fig. 1c for camera
788 locations) showing the crater terrace and flow field during the opening phase of the 2007 effusive eruption.
789 The chronological sequence of the images given in (d-i) tracks emplacement of lava flows fed by the fissure
790 opening on the NE flank of the crater terrace. (a) Location and names of active vents as of 26 February 2007
791 (one day before the start of the 2007 effusive eruption). Red-dashed circle locates vent bN_1 which collapsed
792 the next day. (b) Image acquired during fissure propagation on 27 February 2007. Red-dashed circle
793 indicates location of upslope-propagating fissure, opening between bN_2 and bN_1. Movement on this fissure
794 caused, one minute later, a small failure of the SE rim of vent bN_2. (c) Image showing lava flow extending
795 across the saddle between vents bN_1 and bN_2. (d) Image obtained during the opening of Vent 1 on the NE
796 flank of the crater terrace. The yellow-dotted line outlines the craters and the white-dotted line traces the
797 profile of Pianoro (~650 m a.s.l.). (e) Image showing spreading of the first lava flow (FL1) across the 2002-03
798 lava shield (white-dotted line). (f) Image obtained after flow FL1 had begun to extend down the upper Sciara
799 del Fuoco itself. White arrow indicates the position of the active lava flow front. (g) Image of FL1 spreading
800 across the middle of the Sciara del Fuoco. The location of the active flow front is marked by the red arrow
801 (black arrow shows previous position in (f) - distance between the two arrows is approximately 150 m). (h-i)
802 Images acquired as the flow front extended onto the lower Sciara del Fuoco, where it excavated the ground

[*Calvari et al.,* 2005a, 2005b] producing an increasingly thick ash cloud which obscured visibility, to finally enter the sea. The red square in (g) shows the area imaged in (d-f).

Figure 4 – View from West side of the Sciara del Fuoco at 16:30 on 27 February 2007 showing the first lava flows reaching the sea. Note the eruptive fissure on the NE flank of the crater terrace releasing white steam and gas, and the white columns of steam rising from the lava flow fronts where they meet the sea. Brown dust rising around and above Flow 1 (FL1) result from ground excavation and landslides triggered by lava flow advance. Photo taken from the helicopter of Protezione Civile Regione Siciliana by S. Calvari.

Figure 5 – Sequence of frames recorded by camera SQV400 (see Fig. 1c for location). (a-b) Images of lava flow activity. (c-f) Images charting the initial stages of the opening of Vent 2 (see Fig. 1c for location) in the afternoon of 27 February 2007. Images given in (c-f) also record the emission of the FL4 lava flow, debris flow and associated dust clouds. (g) Graph showing the maximum apparent temperature recorded by camera SQT400 revealing variation due to the pulsing movement of the FL3 front, followed by an increase due to the opening of Vent 2. Maximum temperature is sampled every 10 seconds.

Figure 6 – (a): Photo of the Sciara del Fuoco taken from the NNE during a boat-based survey performed on 5 March 2007 showing Vent 2 and the it's lava flow field (outlined using a dotted red line). The flow has reached the sea to generate thick steam clouds. The yellow box shows the area imaged in (b). (b): Photo of the Sciara del Fuoco taken from the NE during a helicopter survey on 4 March 2007 showing Vent 2 on the eastern Sciara del Fuoco, and the depression above the vent region caused by dike drainage. The line of fume apparent in the upper right of the image marks the eruptive fissure on the NE flank of the crater terrace. The white steaming area below this marks the location of lava flows of erupted during opening phase. Photo's courtesy of Dipartimento di Protezione Civile.

Figure 7 – Sequence of images of the crater terrace recorded by camera SPI between 4 and 7 March 2007 showing widening of the crater rim by repeated collapses. The coloured-dotted lines indicate changes in the position of the crater rim. Increasing darkness and decreasing quality of the images are the result of ash emission during collapses.

Figure 8 – (a): Photo of the Sciara del Fuoco taken from the NW showing the position of Vents 1, 2 and 3, as well as the flow fields that they fed (Vent 1 flow field: black dotted outline; Vent 2 flow field: red dotted outline; Vent 3 flow field: yellow dotted outline). Note the deep elongated depressions above Vents 2 and 3 due to dike drainage. (b): Graph of maximum apparent temperature recorded by camera SQT400 during 9 March (sampling rate is 10 seconds). The increase in temperature at 13:31:49 relates to the opening of Vent 3 at 550 m a.s.l.

Figure 9 – Sequence of images recorded by camera SPI during the 15 March 2007 paroxysm. (a) Image recording pre-explosion collapses from the inner crater walls. (b) Image recording the initial phase of the paroxysm at the NE crater at 20:38:18. (c) Image acquired at 20:38:20 showing explosion source propagation to the Central crater. (d) Image acquired at 20:38:22 showing propagation to the SW crater. (e,

h): The same sequence of events recorded from camera SQT400. From this camera we see the craters from below and from the NE. The first image in the series (e) shows that just a small thermal anomaly was visible from below at the onset of the paroxysm. The second image (f) shows that, when the paroxysm began, two diverging eruptive clouds formed and extended out of the top of the camera field of view. The image in (h) shows three fire fountains from each of the three crater zones and pyroclastic flows spreading up to Bastimento (located using black arrow). (i): Graph of the maximum apparent temperature recorded on 15 March 2007 by camera SQT400 showing the sudden start of the 15 March paroxysm and several peaks caused by fire fountain activity and pyroclastic flows. The thermal signal caused by pyroclastic flows spreading on the Pianoro is highlighted by the arrow.

Figure 10 – (a): Graph plotting effusion rates obtained from thermal camera, AVHRR, and MODIS data, showing high initial values followed by a roughly steady trend punctuated by small pulses. (b): Graph of the maximum and minimum cumulative volumes calculated from data in (a).

Figure 11 – Cross-section sketches of Stromboli (viewed from North) summarizing our interpretation of the chronology of the 2007 effusive eruption. (a): Enhanced magma and gas flux (red) ascends the conduit (brown) during the weeks preceding the onset of the effusive eruption (N, C and S mark the NE, Central and SW craters). (b): The eruptive fissure opens within the NE crater due to increased magmastatic pressure. (c): The eruptive fissure intersects the NE flank of the crater terrace (black line) and Vent 1 (red dot) opens at 650 m a.s.l. to produce a lava flow (purple) that extends to the sea. (d): Magma level within the conduit drops so that Vent 1 and its lava flow becomes inactive (dark grey). The feeder dike propagates down slope along the detachment surface beneath the sliding portion of the SDF (yellow dotted line). Vent 2 opens at 400 m.s.l. to feed lava flow (purple) to the sea. (e): Effusion rate at Vent 2 declines until the vent closes. Magma level within the feeder dike backs up (along the line of the detachment surface - yellow dotted line), and Vent 3 re-opens at 550 m to feed lava flow to the sea. (f): Magma level within the conduit drops causing Vent 3 to close (grey). Magma fills the feeder dike so that Vent 2 becomes active and lava spreads from this vent to the sea.

Figure 12 – (a): Photo taken in August 2003 showing the crater terrace (source of white steam in top right) and the eruptive fissure (red dotted line) that opened on the NE flank of the crater terrace during the 2002-03 effusive eruption. (b): Photo taken in June 2007 from NE showing the two eruptive fissures (red dotted lines) that opened during the 2007 effusive eruption. The positions of Vents 1, 2 and 3 are also marked (yellow dots). The uppermost fissure in (b) is interpreted as the reactivation of the 2002-03 fissure, whereas the lower vents form on the upper boundary of a block that had been sliding since the start of the 2002-03 effusive eruption. The green dotted line marks the boundary of the sliding block, and the green arrow shows its direction of movement. The 2007 effusive Vents (1, 2 and 3, yellow dots) are located along the intersection of the sliding block with topography.

Tables

885 **Table 1** – Effusion rate data from AVHRR and MODIS satellite data and from FLIR helicopter surveys

886

887 **Table 2** – Cumulative volumes calculated from AVHRR, MODIS and FLIR data.

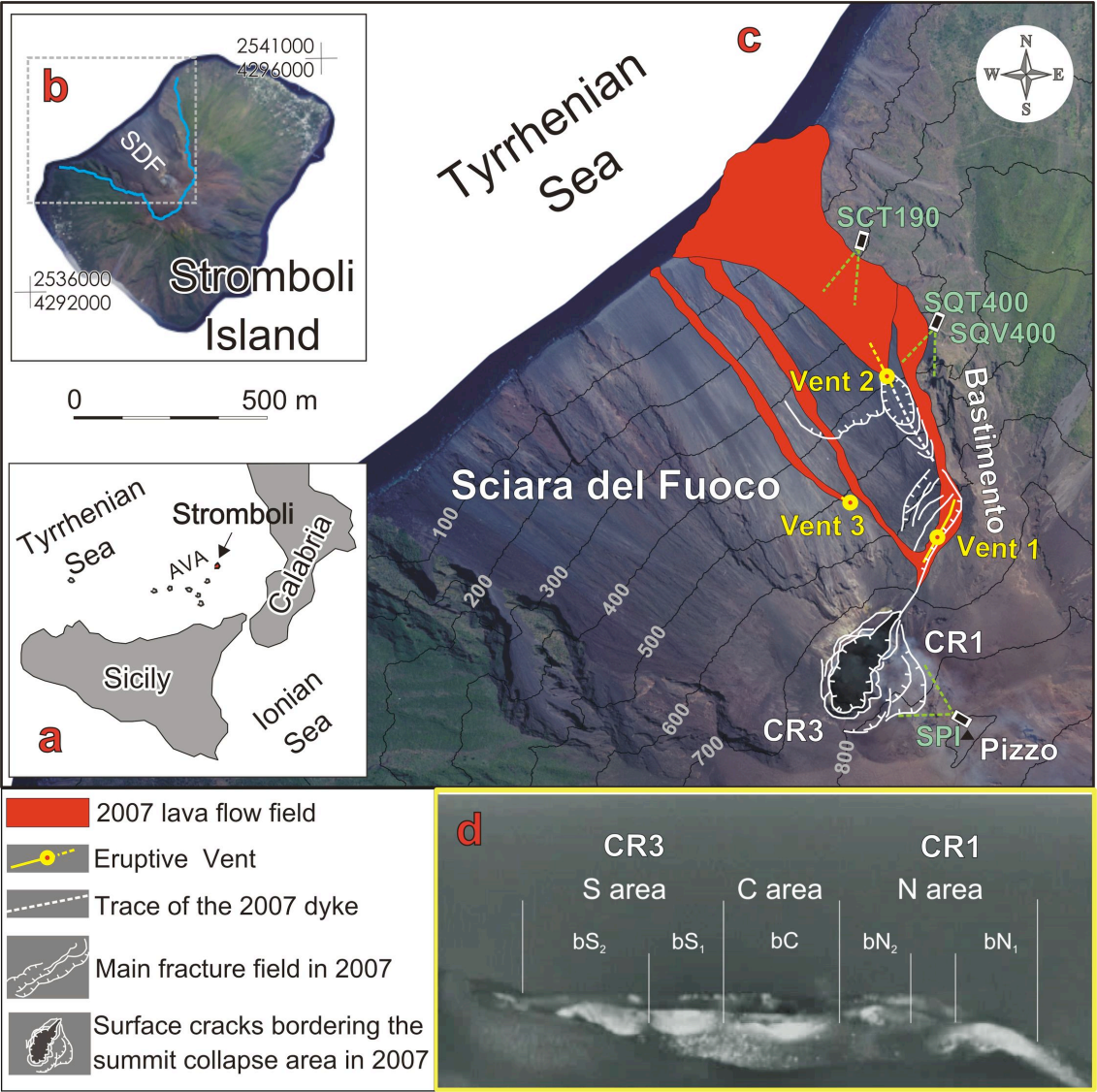
b
2541000
4296000
SDF
2536000
4292000
Stromboli
Island
0
500 m
a
Tyrrhenian
Sea
Stromboli
AVA
Calabria
Sicily
Ionian
Sea
c
Tyrrhenian
Sea
N
W
E
S
SCT190
SQT400
SQV400
Vent 2
Bastimento
Sciara del Fuoco
Vent 3
Vent 1
100
200
300
400
500
600
700
800
CR1
CR3
SPI
Pizzo
2007 lava flow field
Eruptive Vent
Trace of the 2007 dyke
Main fracture field in 2007
Surface cracks bordering the
summit collapse area in 2007
d
CR3
S area
C area
CR1
N area
bS2
bS1
bC
bN2
bN1

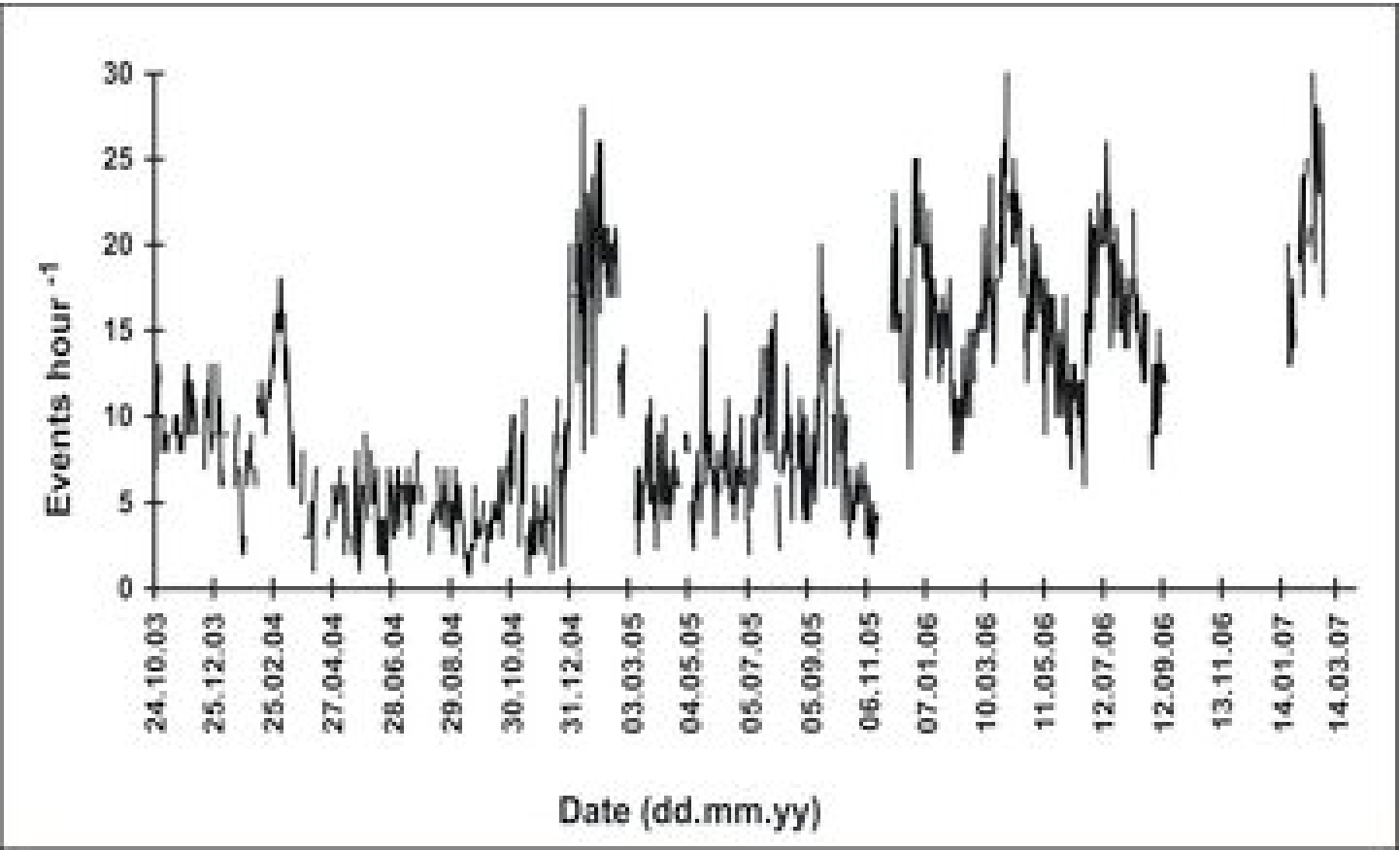
Events hour -1
30
25
20
15
10
5
0
24.10.03
25.12.03
25.02.04
27.04.04
28.06.04
29.08.04
30.10.04
31.12.04
03.03.05
04.05.05
05.07.05
05.09.05
06.11.05
07.01.06
10.03.06
11.05.06
12.07.06
12.09.06
13.11.06
14.01.07
14.03.07
Date (dd.mm.yy)

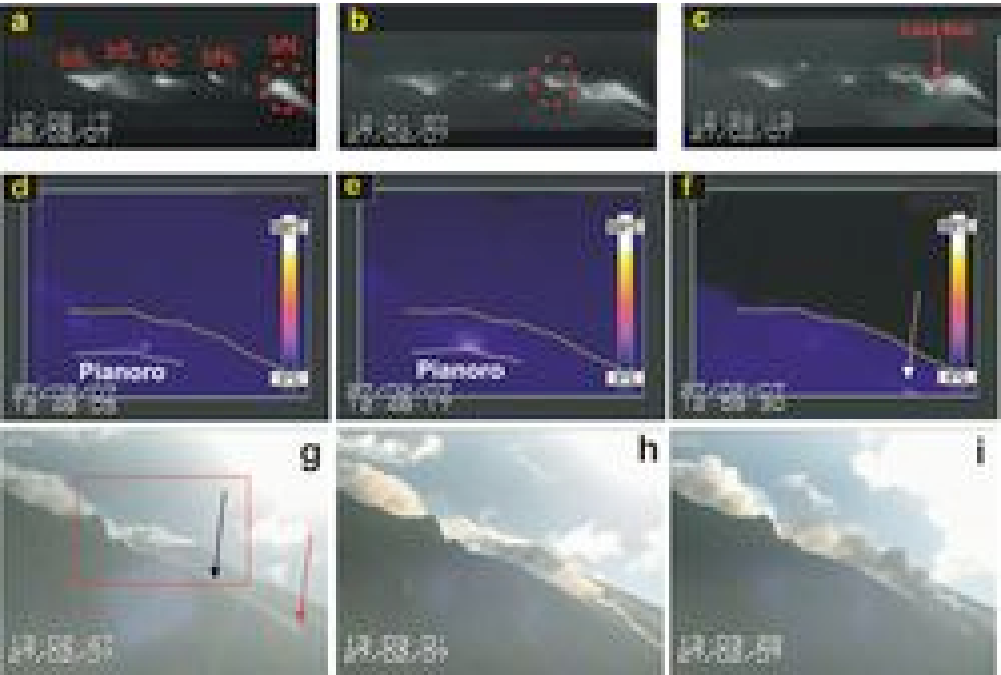
a
b
c
d
Planora
e
Planora
f
g
h
i

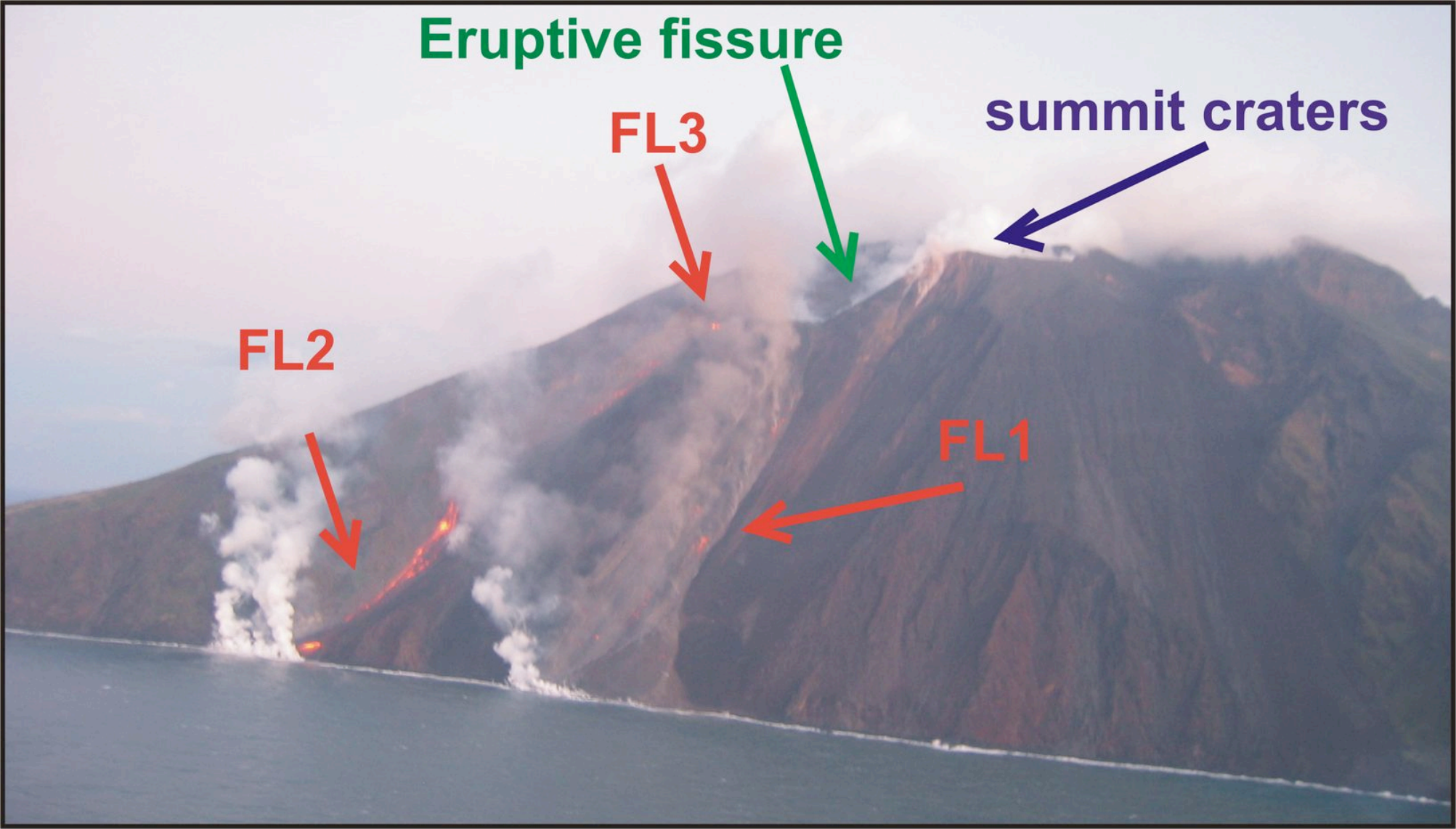
Eruptive fissure
FL3
summit craters
FL2
FL1

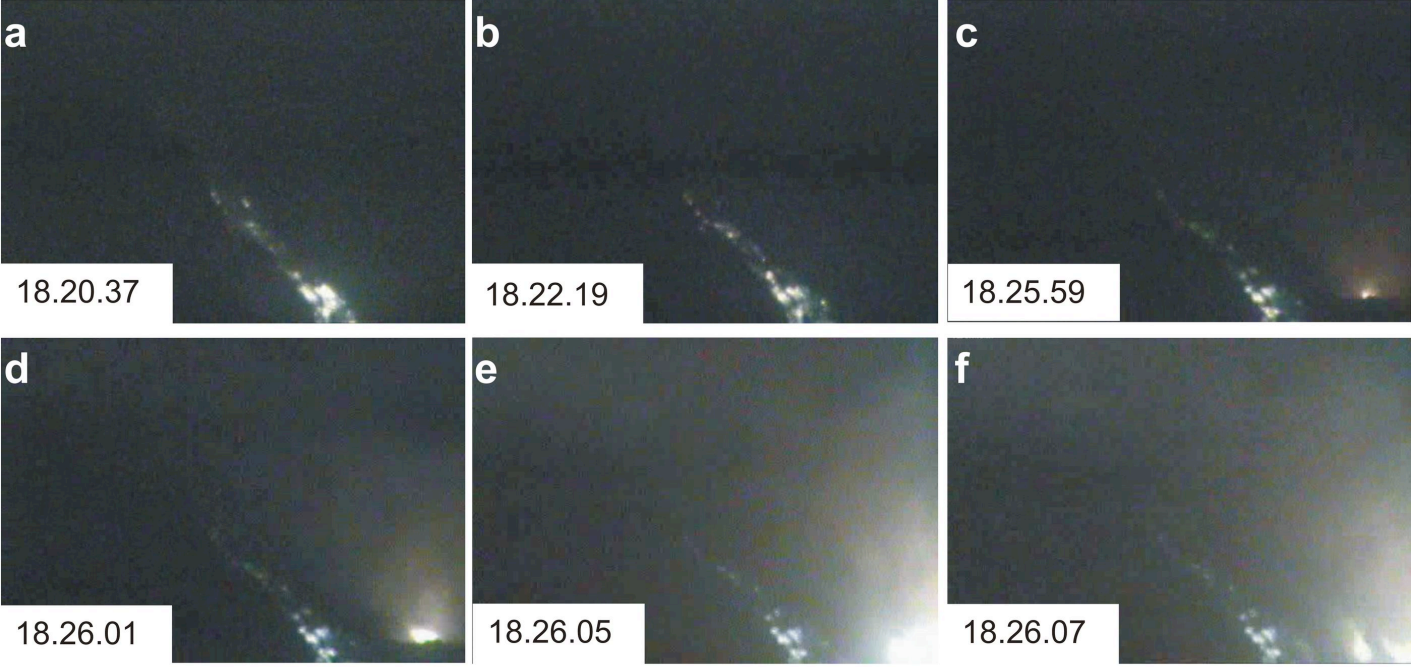
a
18.20.37
b
18.22.19
c
18.25.59
d
18.26.01
e
18.26.05
f
18.26.07

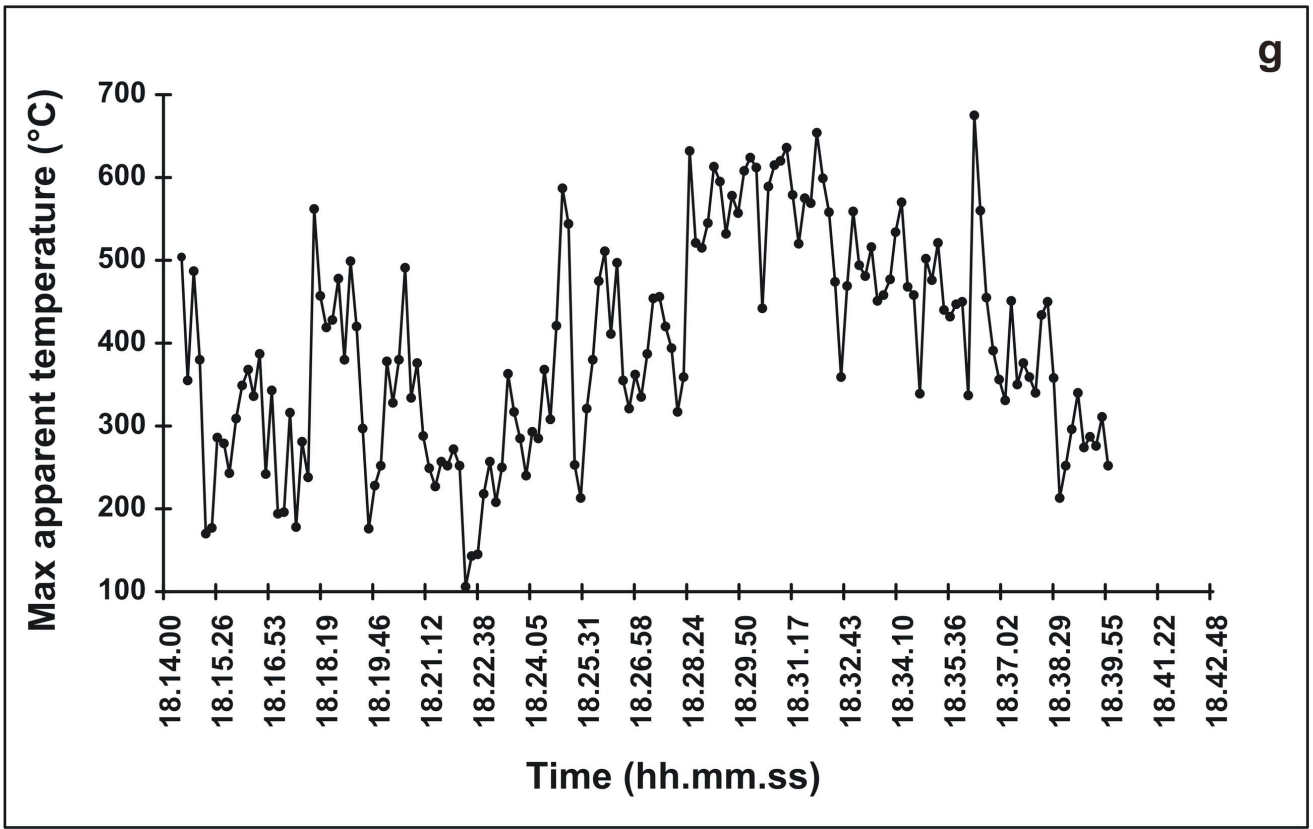
g
Max apparent temperature (°C)
700
600
500
400
300
200
100
18.14.00
18.15.26
18.16.53
18.18.19
18.19.46
18.21.12
18.22.38
18.24.05
18.25.31
18.26.58
18.28.24
18.29.50
18.31.17
18.32.43
18.34.10
18.35.36
18.37.02
18.38.29
18.39.55
18.41.22
18.42.48
Time (hh.mm.ss)

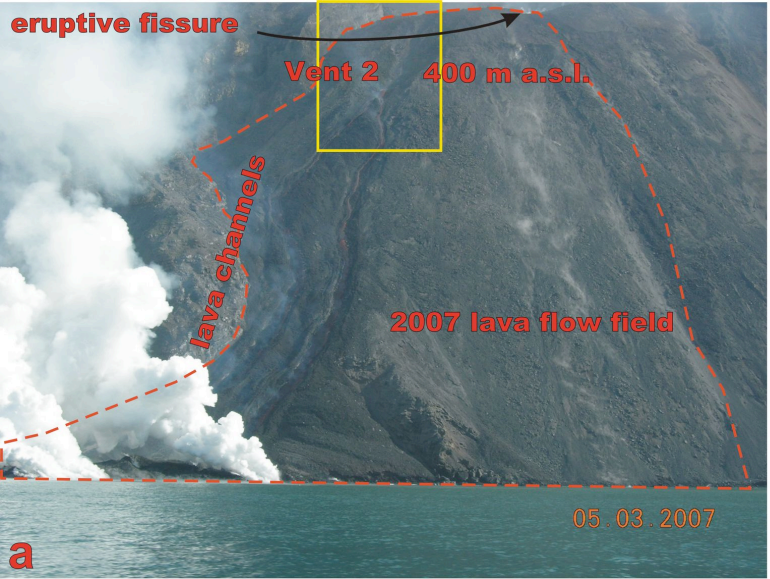
eruptive fissure
Vent 2
400 m a.s.l.
lava channels
2007 lava flow field
05.03.2007
a


eruptive fissure
drained dike
Vent 2
400 m a.s.l.
b

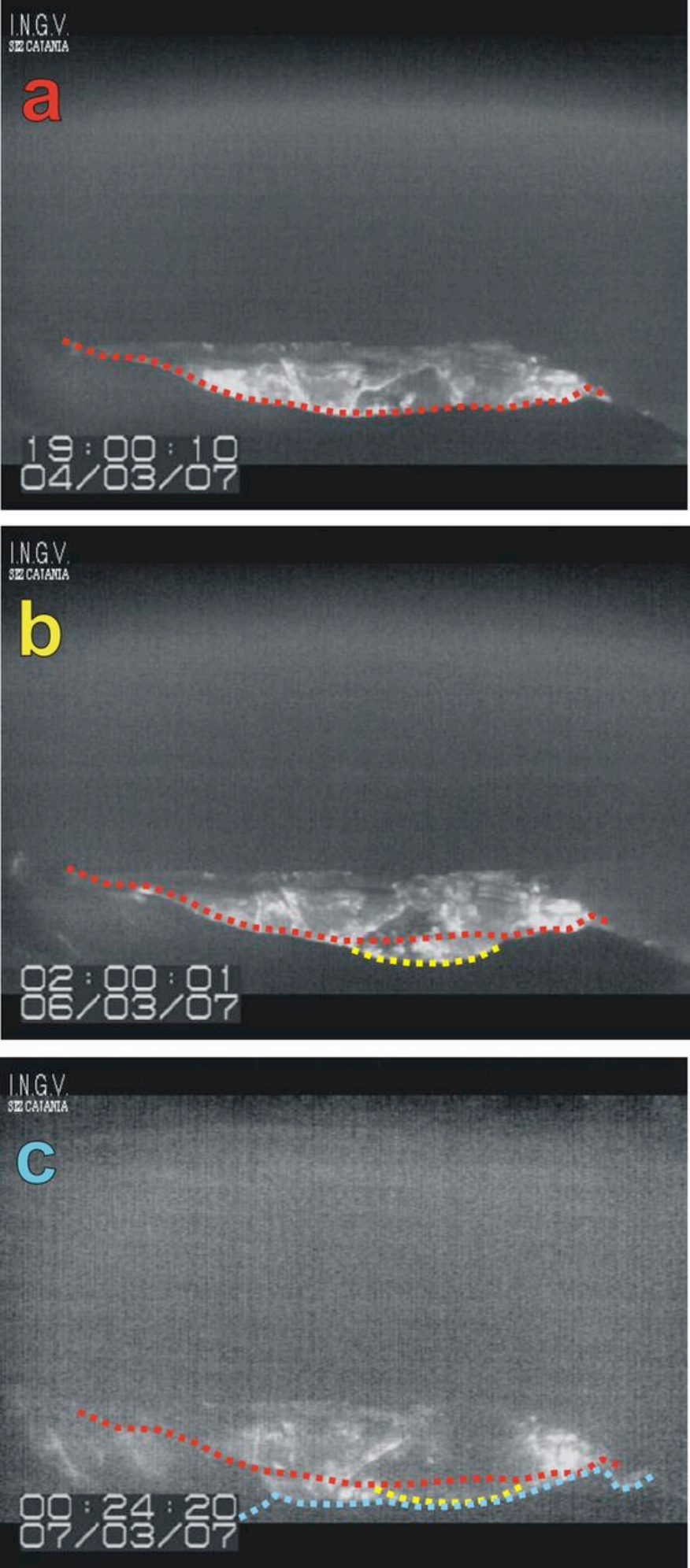
I.N.G.V.
SEZ CATANIA
a
19:00:10
04/03/07
I.N.G.V.
SEZ CATANIA
b
02:00:01
06/03/07
I.N.G.V.
SEZ CATANIA
c
00:24:20
07/03/07

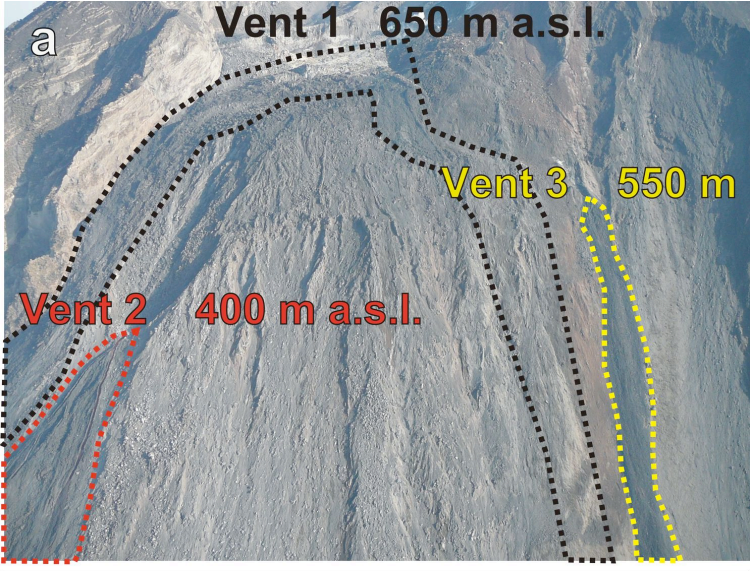
a
Vent 1 650 m a.s.l.
Vent 3 550 m
Vent 2 400 m a.s.l.

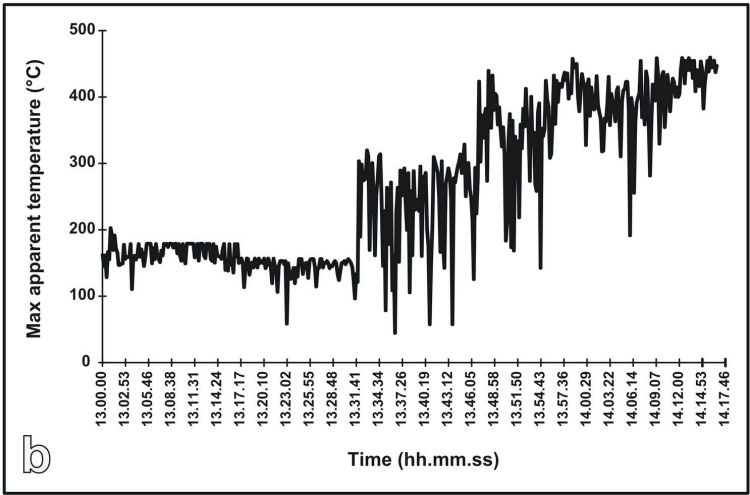
b
Max apparent temperature (°C)
0
100
200
300
400
500
13.00.00
13.02.53
13.05.46
13.08.38
13.11.31
13.14.24
13.17.17
13.20.10
13.23.02
13.25.55
13.28.48
13.31.41
13.34.34
13.37.26
13.40.19
13.43.12
13.46.05
13.48.58
13.51.50
13.54.43
13.57.36
14.00.29
14.03.22
14.06.14
14.09.07
14.12.00
14.14.53
14.17.46
Time (hh.mm.ss)

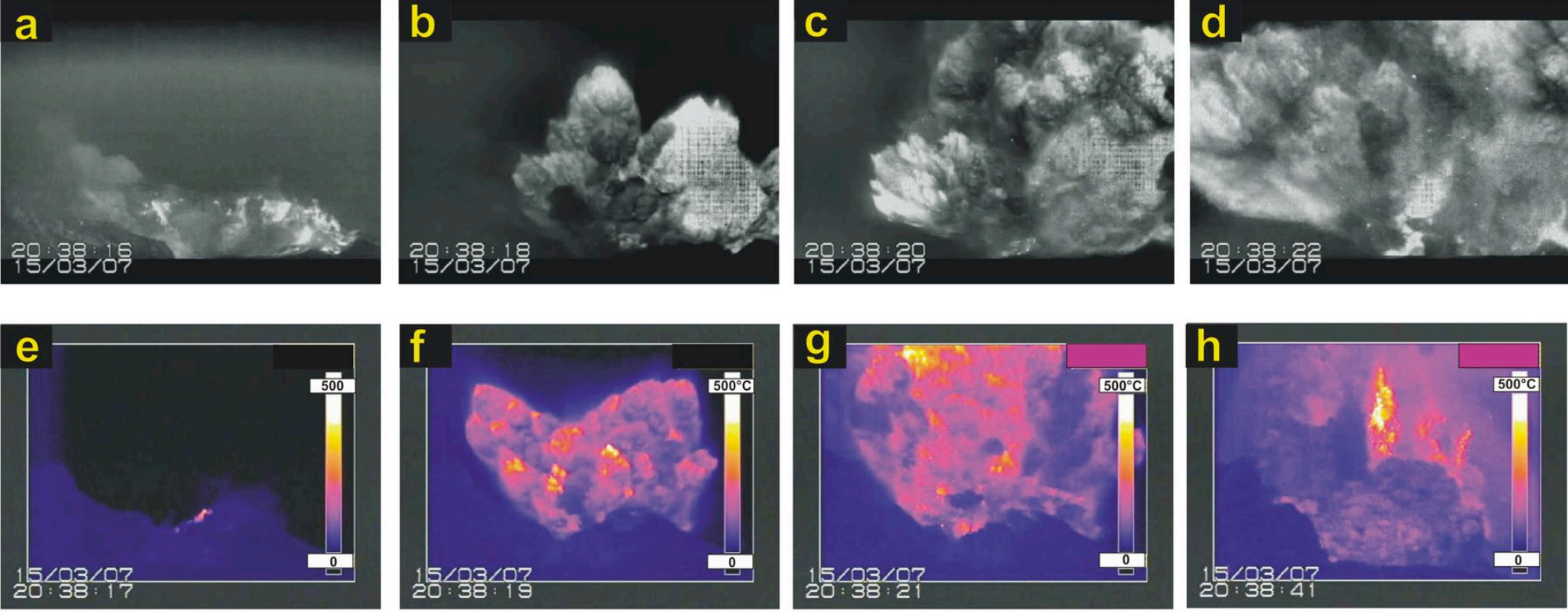
a
20:38:16
15/03/07
b
20:38:18
15/03/07
c
20:38:20
15/03/07
d
20:38:22
15/03/07
e
500
0
15/03/07
20:38:17
f
500°C
0
15/03/07
20:38:19
g
500°C
0
15/03/07
20:38:21
h
500°C
0
15/03/07
20:38:41

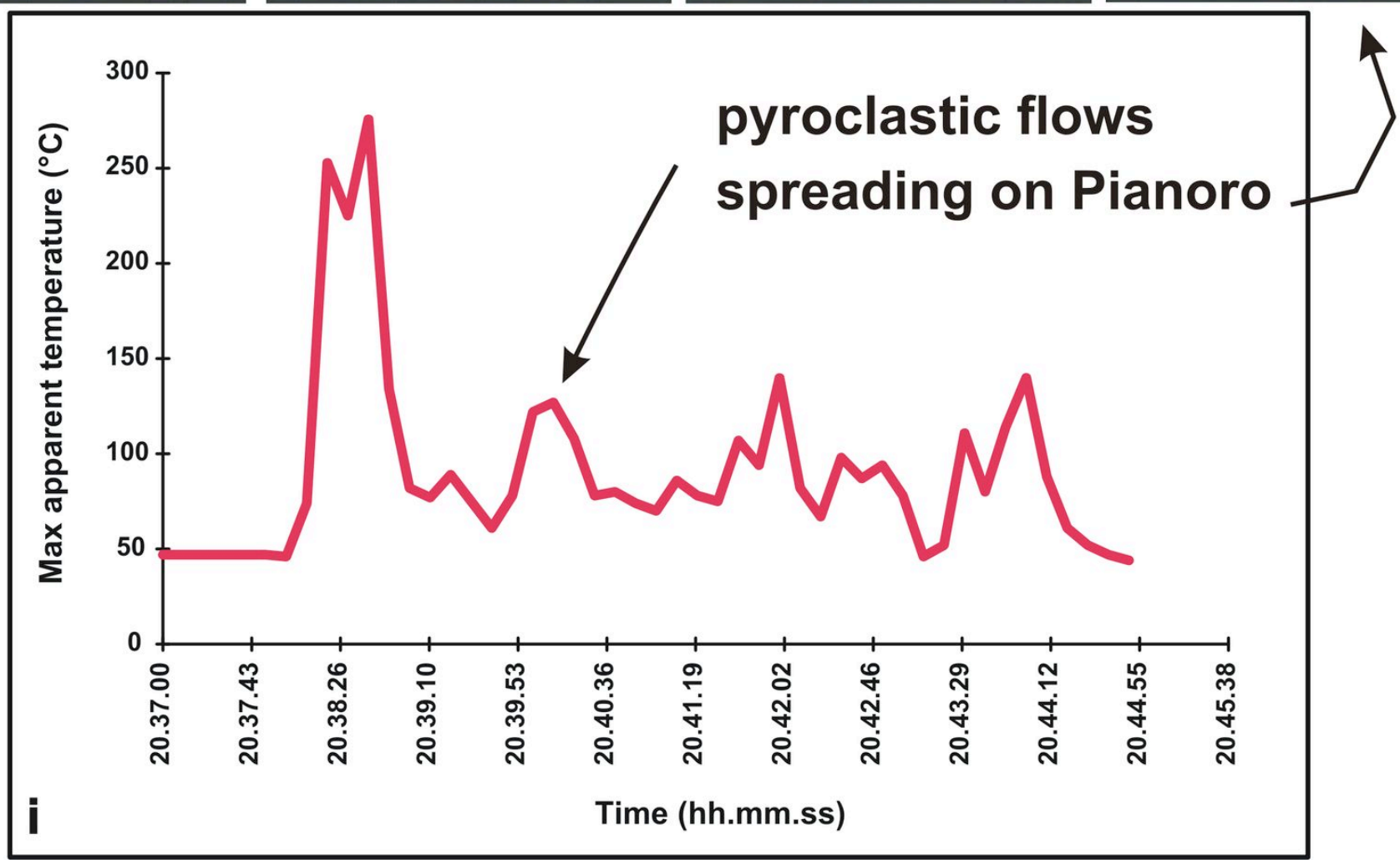
pyroclastic flows
spreading on Pianoro
Max apparent temperature (°C)
300
250
200
150
100
50
0
20.37.00
20.37.43
20.38.26
20.39.10
20.39.53
20.40.36
20.41.19
20.42.02
20.42.46
20.43.29
20.44.12
20.44.55
20.45.38
Time (hh.mm.ss)
i

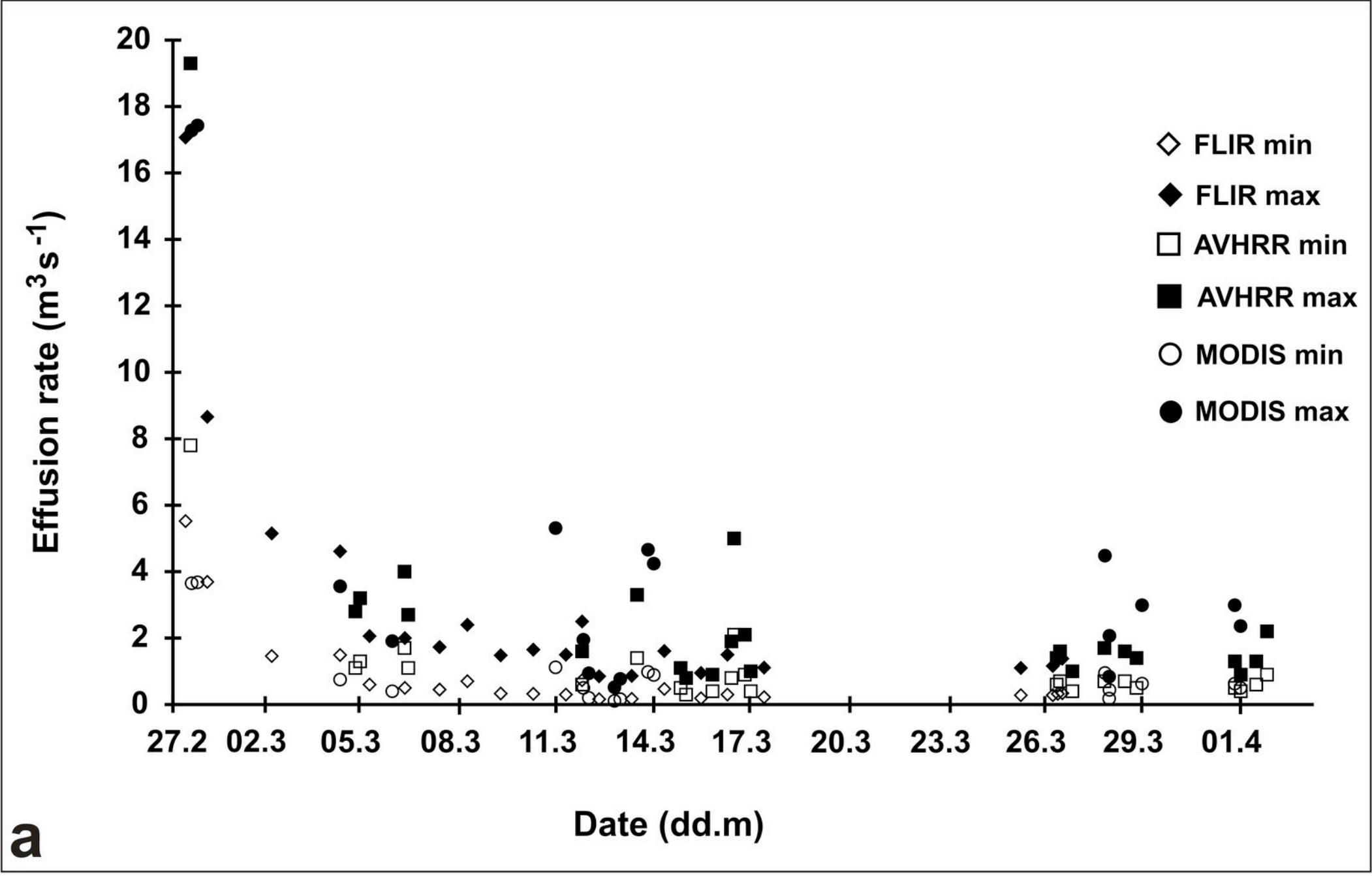
20
18
16
14
12
10
8
6
4
2
0
Effusion rate (m^3s^{-1})
FLIR min
FLIR max
AVHRR min
AVHRR max
MODIS min
MODIS max
27.2
02.3
05.3
08.3
11.3
14.3
17.3
20.3
23.3
26.3
29.3
01.4
Date (dd.m)
a

AVHRR
MODIS
FLIR
7.0
6.0
5.0
4.0
3.0
2.0
1.0
0.0
Cumulative volume (10^6m^3)
27.2
28.2
01.3
02.3
03.3
04.3
05.3
06.3
07.3
Date (dd.m)
b

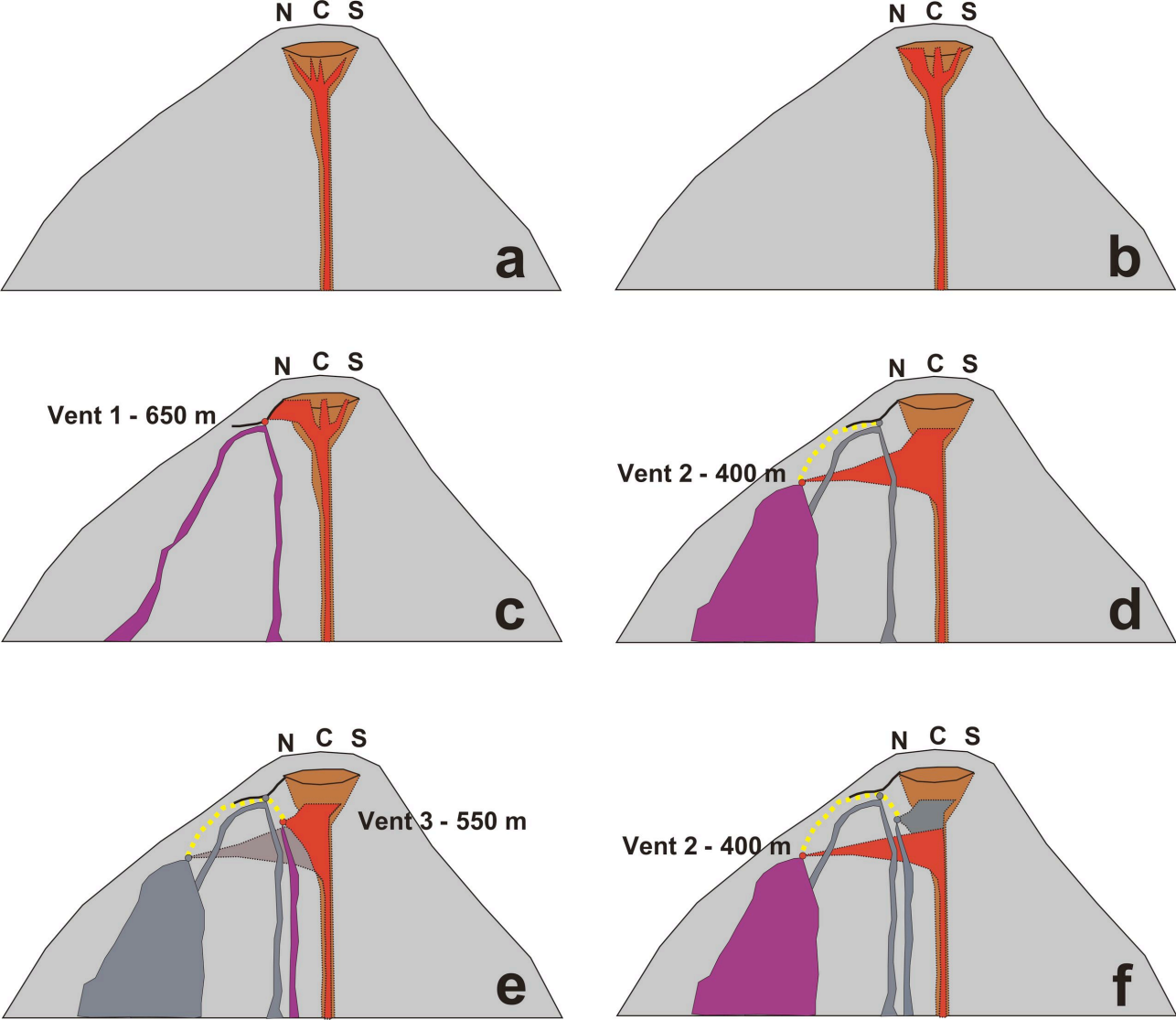
N C S
a
N C S
b
N C S
Vent 1 - 650 m
c
N C S
Vent 2 - 400 m
d
N C S
Vent 3 - 550 m
e
N C S
Vent 2 - 400 m
f

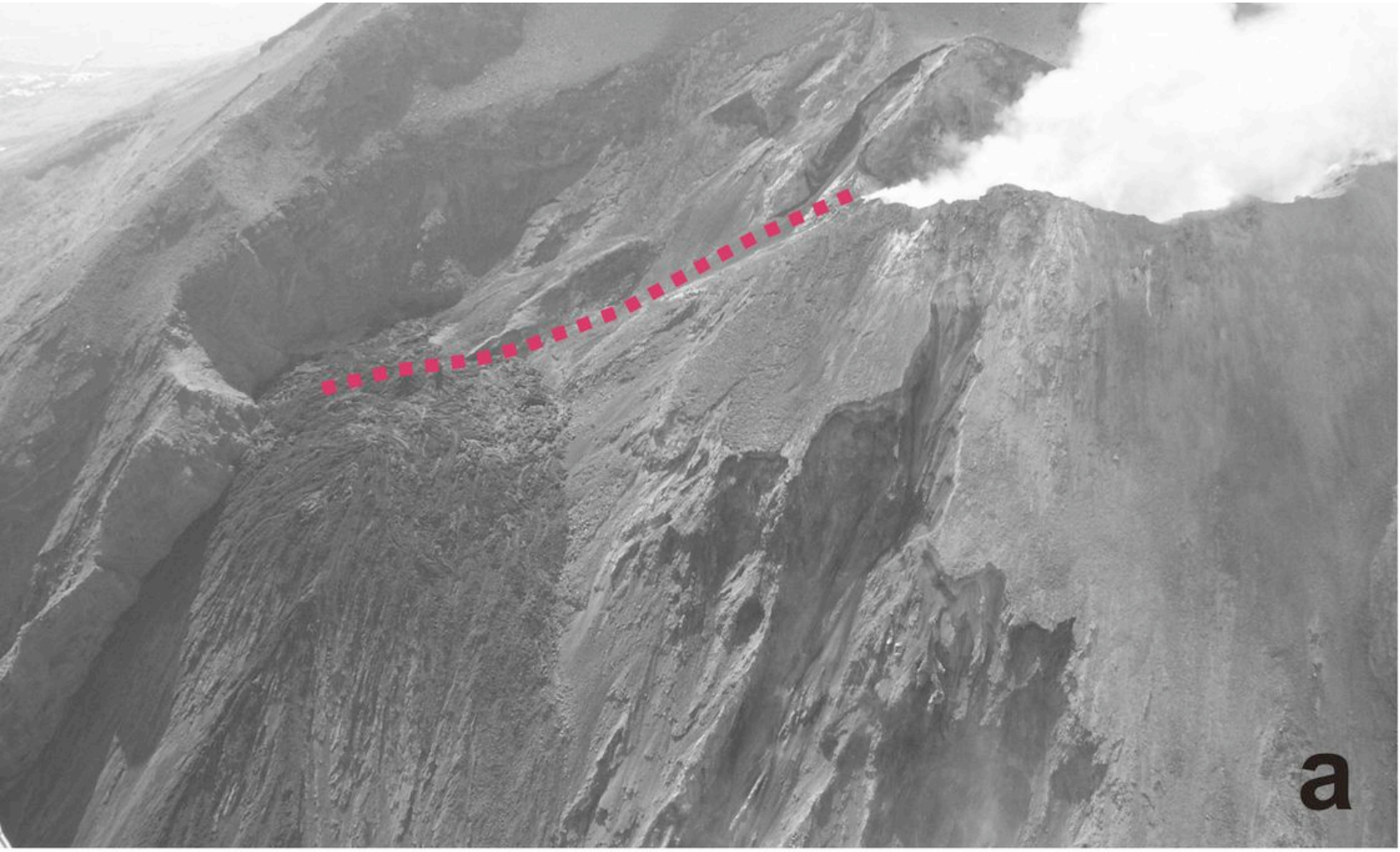
a

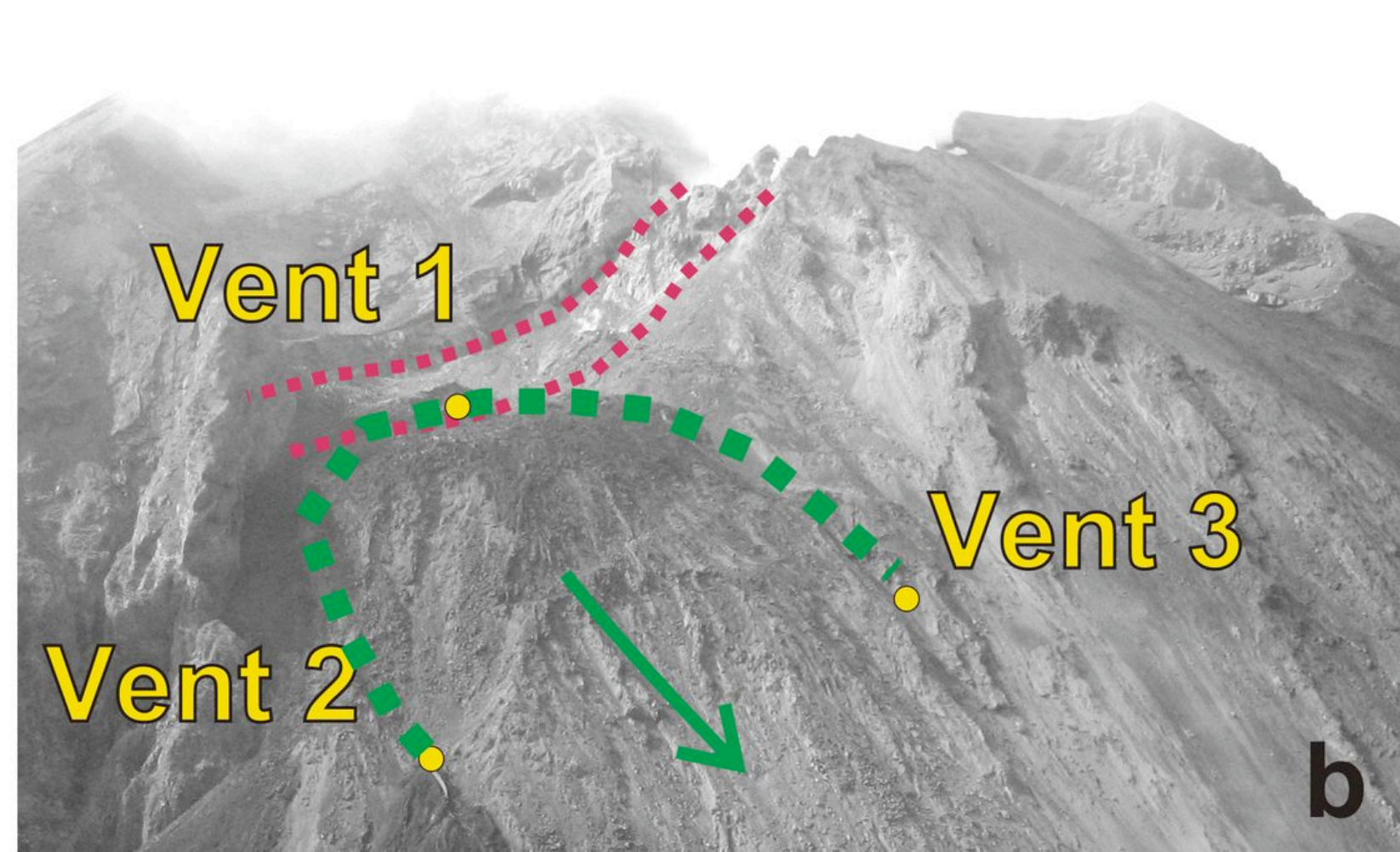
Vent 1
Vent 3
Vent 2
b

Date dd/mm	Time hh/mm	AVHRR min $m^3 s^{-1}$	AVHRR max $m^3 s^{-1}$	AVHRR mean $m^3 s^{-1}$	MODIS min $m^3 s^{-1}$	MODIS max $m^3 s^{-1}$	MODIS mean $m^3 s^{-1}$	FLIR min $m^3 s^{-1}$	FLIR max $m^3 s^{-1}$	FLIR mean $m^3 s^{-1}$
27/02	16.30							5.52	17.07	11.30 ± 5.78
27/02	20.06	7.8	19.3	13.55±5.75						
27/02	21.00				3.65	17.28	10.46±6.8			
28/02	1.15				3.68	17.43	10.55±6.8			
28/02	8.30							3.69	8.66	6.18 ± 2.49
02/03	8.00							1.46	5.15	3.31±1.85
04/03	10.15				0.75	3.56	2.1±1.04	1.49	4.61	3.05±1.56
04/03	21.31	1.1	2.8	1.65±0.85						
05/03	1.01	1.3	3.2	2.25±0.95						
05/03	8.00							0.60	2.06	1.33±0.73
06/03	0.40				0.4	1.91	1.15±0.75			
06/03	9.41	1.7	4	2.85±1.15						
06/03	10.00							0.50	2.00	1.25±0.75
06/03	12.26	1.1	2.7	1.9±0.8						
07/03	11.30							0.45	1.73	1.09±0.64
08/03	8.00							0.70	2.40	1.55±0.85
09/03	8.30							0.33	1.48	0.91±0.58
10/03	8.30							0.32	1.65	0.99±0.67
11/03	0.55				1.12	5.31	3.21±2.1			
11/03	8.30							0.73	2.50	1.6±0.89
11/03	20.29	0.6	1.6	1.1±0.5						
11/03	21.25				0.5	1.95	1.2±0.7			
12/03	1.25				0.2	0.94				
12/03	9.00							0.16	0.85	0.51±0.35
12/03	20.20				0.11	0.52	0.31±0.2			
13/03	0.30				0.16	0.77	0.46±0.3			
13/03	9.00							0.17	0.86	0.52±0.35
13/03	12.55	1.4	3.3	2.35±0.95						
13/03	21.00				0.98	4.66	2.82±1.8			
14/03	1.15				0.89	4.24	2.5±1.6			
14/03	9.00							0.47	1.61	1.04±0.57
14/03	21.00	0.5	1.1	0.8±0.3						
15/03	12.00							0.19	0.95	0.57±0.38
15/03	20.27	0.4	0.9	0.65±0.25						
16/03	7.30							0.30	1.50	0.90±0.60
16/03	10.25	0.8	1.9	1.35±0.55						
16/03	12.24	2.1	5	3.55±1.45						
16/03	20.14	0.9	2.1	1.5±0.6						
17/03	0.37	0.4	1	0.7±0.3						
17/03	10.30							0.22	1.11	0.67±0.45
25/03	7.30							0.28	1.10	0.69±0.41
26/03	7.00							0.28	1.16	0.72 ± 0.44
26/03	9.54	0.6	1.4	1±0.4						
26/03	10.45							0.32	1.34	0.83 ± 0.51
26/03	12.21	0.7	1.6	1.15±0.25						
26/03	14.00							0.34	1.38	0.86 ± 0.52
26/03	21.23	0.4	1	0.7±0.3						
27/03	21.00	0.7	1.7	1.2±0.5						
27/03	21.25				0.95	4.48	2.75±1.76			
28/03	0.30				0.18	0.84	0.51±0.33			
28/03	0.45				0.44	2.07	1.25±0.8			
28/03	12.01	0.7	1.6	1.15±0.45						
28/03	20.37	0.5	1.4							
29/03	0.45				0.63	2.99	1.81±1.18			
30/03	14.00									
31/03	21.00				0.63	2.99	1.81±1.20			
31/03	21.08	0.5	1.3	0.9±0.4						
01/04	1.15				0.5	2.36	1.43±0.93			
01/04	1.24	0.4	0.9	0.65±0.25						
01/04	12.50	0.6	1.3	0.95±0.35						
01/04	20.45	0.9	2.2	1.55±0.65						

Date dd/mm	time hh:mm	AVHRR max cum. vol. 10^6 m^3	AVHRR min cum. vol. 10^6 m^3	MODIS max cum. vol. 10^6 m^3	MODIS min cum. vol. 10^6 m^3	FLIR max cum. vol. 10^6 m^3	FLIR min cum. vol. 10^6 m^3
27/02	16:30					1.01	0.33
27/02	20:06	1.40	0.56				
27/02	21:00			1.31	0.27		
28/02	1:15			1.57	0.33		
28/02	8:30					1.75	0.59
2/03	8:00					2.94	1.03
4/03	10:15			5.54	1.17	3.82	1.30
4/03	21:31	6.23	2.51				
5/03	1:01	6.26	2.52				
5/03	8:00					4.08	1.38
6/03	0:40			5.92	1.25		
6/03	9:41	6.69	2.70				
6/03	10:00					4.27	1.43
6/03	12:26	6.72	2.71				
7/03	11:30					4.44	1.48
7/03	16:30					4.47	1.49
8/03	8:00					4.59	1.52
9/03	8:30					4.76	1.56
10/03	8:30					4.89	1.59
11/03	0:55			7.48	1.58		
11/03	8:30					5.03	1.62
11/03	17:30					5.09	1.63
11/03	20:29	7.71	3.11				
11/03	21:25			7.75	1.64		
12/03	1:25			7.77	1.64		
12/03	9:00					5.19	1.66
12/03	20:20			7.82	1.65		
13/03	0:30			7.83	1.66		
13/03	9:00					5.26	1.67
13/03	12:55	8.06	3.26				
13/03	21:00			8.03	1.70		
14/03	1:09	8.28	3.35				
14/03	1:15			8.10	1.71		
14/03	9:00					5.37	1.70
14/03	21:00	8.32	3.36				
15/03	00:58	8.32	3.36				
15/03	12:00					5.49	1.73
15/03	20:27	8.38	3.38				
16/03	7:30					5.58	1.75
16/03	10:25	8.45	3.41				
16/03	12:24	8.47	3.42				
16/03	20:14	8.57	3.47				
17/03	0:37	8.60	3.48				
17/03	10:30					5.71	1.78
25/03	7:30					6.46	1.95
26/03	7:00					6.55	1.97
26/03	9:54	9.57	3.88				
26/03	10:45					6.57	1.97
26/03	12:21	9.58	3.89				
26/03	14:00					6.59	1.98
26/03	21:23	9.62	3.91				
27/03	21:00	9.74	3.95				
27/03	21:25			13.3	2.81		
28/03	0:30			13.3	2.82		
28/03	0:45			13.3	2.82		
28/03	12:01	9.83	3.99				
28/03	20:37	9.87	4.01				
29/03	0:45			13.6	2.87		
30/03	14:00						
31/03	21:00			14.3	3.02		
31/03	21:08	10.2	4.14				
1/04	1:15			14.3	3.03		
1/04	1:24	10.2	4.15				
1/04	12:50	10.3	4.17				
1/04	20:45	10.3	4.19				